CORRECTION OF LASER RANGING DATA FOR THE EFFECTS OF HORIZONTAL REFRACTIVITY GRADIENTS

by

C. S. Gardner
B. E. Hendrickson

RRL Publication No. 478

Draft
(Final Report)
December 1976

Supported by

Contract No. NASA NSG 5049

NATIONAL AERONAUTICS & SPACE ADMINISTRATION
Goddard Space Flight Center
Greenbelt, Maryland 20771

RADIO RESEARCH LABORATORY
DEPARTMENT OF ELECTRICAL ENGINEERING
COLLEGE OF ENGINEERING
UNIVERSITY OF ILLINOIS
URBANA, ILLINOIS 61801

UILU-ENG-77-2539

CORRECTION OF LASER RANGING DATA FOR THE EFFECTS OF HORIZONTAL REFRACTIVITY GRADIENTS

by

C. S. Gardner
B. E. Hendrickson

RRL Publication No. 478

Draft
(Final Report)
December 1976

Supported by

Contract No. NASA NSG 5049

NATIONAL AERONAUTICS & SPACE ADMINISTRATION
Goddard Space Flight Center
Greenbelt, Maryland 20771

RADIO RESEARCH LABORATORY
DEPARTMENT OF ELECTRICAL ENGINEERING
COLLEGE OF ENGINEERING
UNIVERSITY OF ILLINOIS
URBANA, ILLINOIS 61801

ABSTRACT

A formula has been developed to correct laser ranging data for the effects of horizontal refractivity gradients. The formula requires the values of the horizontal pressure and temperature gradients at the laser site. The accuracy of this technique was evaluated by comparing the formula with range corrections which were computed by ray tracing.

TABLE OF CONTENTS

I. INTRODUCTION

In recent years laser ranging systems have begun to play an important role in the accurate determination of satellite orbits. For many applications, such as monitoring crustal movements of the earth, position accuracies of several centimeters or less are desirable. Atmospheric refraction may, however, increase the optical path length to an orbiting satellite by over ten meters at low elevation angles.

Various formulas have been proposed to correct laser ranging data for the effects of atmospheric refraction. Based on the work of Marini [3] and Saastamoinen [2], Marini and Murray [1] derived a correction formula which is attractive for satellite ranging applications because it requires only surface measurements of pressure, temperature, and relative humidity. The accuracy of their formula was tested by comparing it with range corrections calculated by ray tracing through atmospheric refractivity profiles. The profiles were generated from radiosonde measurements of pressure, temperature, and relative humidity.

Marini and Murray's formula was derived by assuming that a spherically symmetric refractivity profile adequately characterized the atmosphere. Zanter, Gardner, and Rao [4] and Gardner and Rowlett [6] investigated the validity of this assumption by ray tracing through three-dimensional refractivity profiles. Their results indicate that horizontal refractivity gradients can introduce range errors of over three centimeters at the lower elevation angles (10° - 20°). In this report a correction formula which partially compensates for these gradient effects is derived. The accuracy of the formula is investigated by comparing it with range corrections calculated by ray tracing.

II. CORRECTION FORMULA DERIVATION

Numerous formulas have been developed which partially correct laser satellite ranging measurements for the effects of atmospheric refraction. For many applications such as the monitoring of continental drift, fault motion and other tectonic processes, position accuracies of better than a few centimeters are required. Only the correction formulas developed by Saastamoinen [2] and Marini and Murray [1] provide this accuracy at elevation angles of 10 to 20 degrees. These formulas were derived under the assumption that atmospheric refractivity is spherically symmetric. This assumption holds only approximately even for the normal state of the troposphere. The refractivity at sea level inevitably increases from the warmer equatorial regions toward the colder climates at the poles. In the lower troposphere the surfaces of constant refractivity acquire a general slope toward the equator unless this is prevent . by some local perturbation.

The optical path length will therefore be affected by the horizontal refractivity gradients. These effects are illustrated in ray-trace corrections reported by Zanter, Gardner, and Rao [4] and Gardner and Rowlett [6]. The results indicate refractivity gradients induce changes in the optical path length of as much as four to five centimeters at ten degrees elevation.

Correction formulas which compensate for the horizontal gradients can be derived following an approach similar to Marini and Murray's [1]. The geometry of the laser ranging site and satellite target is shown in Fig. 1. The optical path length between the site and target is defined as the integral of the group refractive index along the ray path. If the refractivity is spherically symmetric, the ray path will lie entirely in a

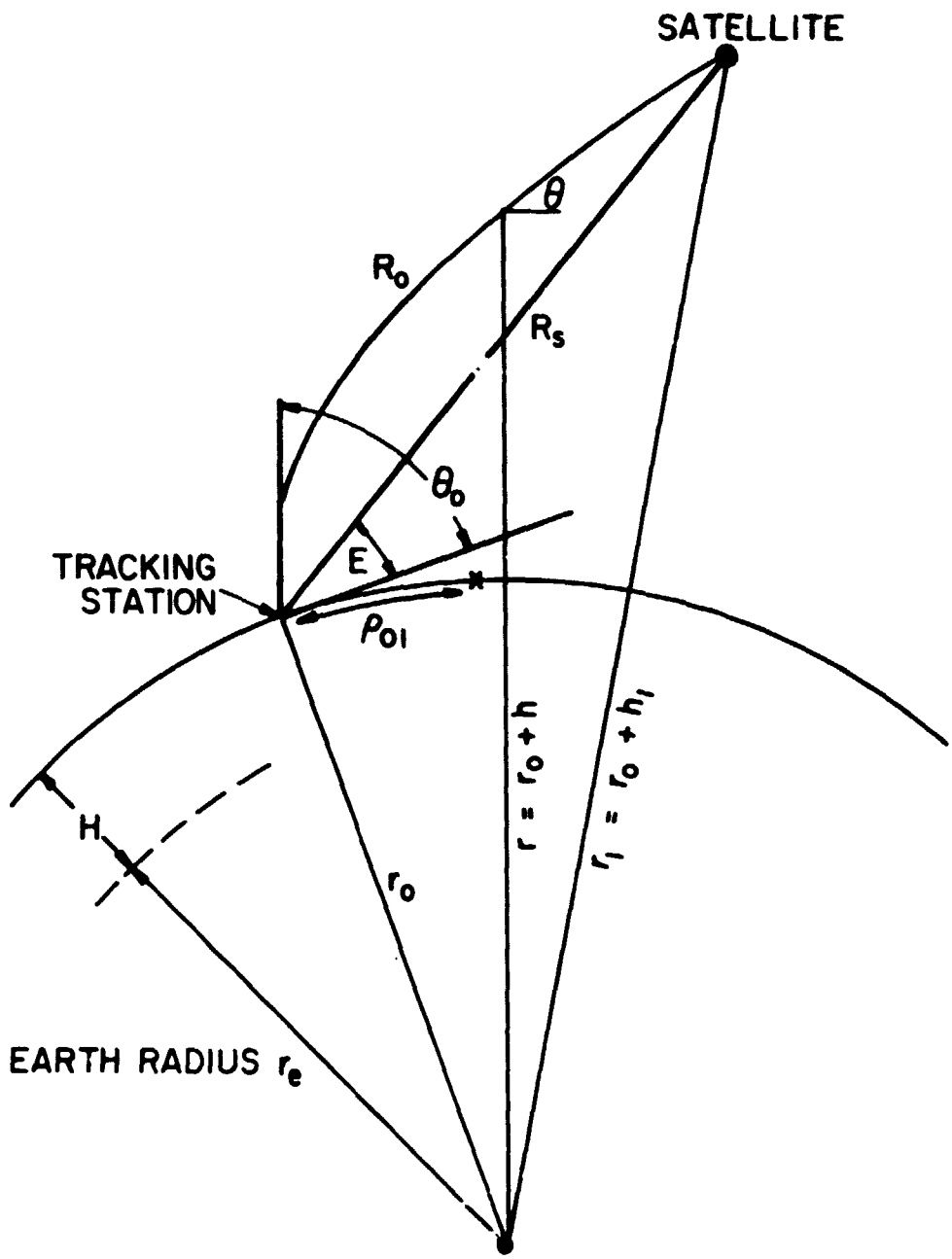

Figure 1. Geometry of ranging site, target, and auxiliary site.

plane. In this case the apparent range measured by a pulsed laser system is given by

$$R_0 = \int_{r_0}^{r_1} dr \frac{n_g}{\sin \theta} \tag{2-1}$$

where n_g is the group index of refraction and θ is given by Snell's law for a spherically stratified medium (see Fig. 1)

$$nr \cos \theta = n_0 r_0 \cos \theta_0 \quad . \tag{2-2}$$

n_0 is the phase refractive index at the laser site.

The range error is the difference between the optical range R_0 and the straight-line path length R_s. If n_g is expressed in terms of the group refractivity N_g,

$$n_g = 1 + 10^{-6} N_g \quad , \tag{2-3}$$

then the range error can be written in the form

$$\Delta R = R_0 - R_s = 10^{-6} \int_{r_0}^{r_1} dr \frac{N_g}{\sin \theta} + \left[\int_{r_0}^{r_1} \frac{dr}{\sin \theta} - R_s \right] \quad . \tag{2-4}$$

The first term is the velocity error while the bracketed term is the difference between the geometric lengths of the ray and straight-line paths.

Since the refractivity gradients are small (see Zanter, Gardner, and Rao [4] and Gardner and Rowlett [6]), we will assume the change in the ray path is slight so that we need only consider the first integral in (2-4). N_g is expanded in a one-dimensional Taylor series about the laser site

$$N_g(h,\rho) = N_g + \rho \frac{\partial}{\partial \rho} N_g\Big|_{\rho=0} + \frac{\rho^2}{2!} \frac{\partial^2}{\partial \rho^2} N_g\Big|_{\rho=0} + \ldots \tag{2-5}$$

where h is the altitude above the laser site and ρ is the horizontal coordinate measured from the ranging site in the direction of the laser beam trajectory. The geometry of the problem is illustrated in Fig. 1. Substituting (2-5) into (2-4) gives

$$\Delta R = SC + GC \tag{2-6}$$

$$SC = 10^{-6} \int_{r_0}^{r_1} dr \frac{N_g(h,0)}{\sin \theta} + \left[\int_{r_0}^{r_1} \frac{dr}{\sin \theta} - R_s \right] \tag{2-7}$$

$$GC = \sum_{k=1}^{\infty} GC_k = 10^{-6} \sum_{k=1}^{\infty} \int_{r_0}^{r_1} dr \frac{N_g^{(k)}(h,0)\rho^k}{k! \sin \theta} \tag{2-8}$$

where

$$N_g^{(k)}(h,0) = \frac{\partial^k}{\partial \rho^k} N_g(h,\rho)\Big|_{\rho=0} .$$

SC is a Marini and Murray-type correction which corresponds to a spherically symmetric atmosphere. The gradient correction term (GC) includes the effects of the horizontal refractivity gradients.

Again, since the horizontal gradients are small, we will approximate GC by the first term in the series, GC_1. The second term, GC_2, will be evaluated approximately to obtain a bound on the error introduced by the neglect of the higher-order terms. The problem is simplified by taking the ρ derivative after the r integral is evaluated

$$GC_1 = 10^{-6} \left[\frac{\partial}{\partial \rho'} \int_{r_0}^{r_1} dr \frac{N_g(h,\rho')\rho}{\sin \theta} \right]\Bigg|_{\rho'=0} . \tag{2-9}$$

The optical group refractivity is given by Marini and Murray [1] as

$$N_g = 80.343\, f(\lambda)\, \frac{P}{T} - 11.3\, \frac{e}{T} \tag{2-10}$$

where

$$e = \frac{Rh}{100} \times 6.11 \times 10^{\frac{7.5(T - 273.15)}{237.3 + (T - 273.15)}} \tag{2-11}$$

$$f(\lambda) = .9650 + \frac{.0164}{\lambda^2} + \frac{.000228}{\lambda^4} \tag{2-12}$$

P = atmospheric pressure (mb)

T = temperature (°K)

e = partial pressure of water vapor (mb)

λ = optical wavelength in microns (530 for this investigation)

Rh = relative humidity (%).

The water vapor contribution is small and can be neglected in the evaluation of $G\dot{v}_1$*. The variation of N_g with altitude can be determined by assuming the atmosphere is in hydrostatic equilibrium. From the perfect-gas law, the law of partial pressures, and the hydrostatic equation, we obtain

$$-\frac{dP}{dh} = \frac{Mg(P - e)}{RT} + \frac{M_w ge}{RT} \simeq \frac{MgP}{RT} \tag{2-13}$$

where

M = 28.966 = molecular weight of dry air

M_w = 18.016 = molecular weight of water vapor

R = 8314.36 joules $(°K)^{-1}(kg\text{-}mole)^{-1}$ = universal gas constant

g = acceleration of gravity (m/sec).

The pressure is obtained by integrating (2-13)

$$P = P_s \exp\left(\frac{-Mg}{R} \int \frac{1}{T}\, dh\right) . \tag{2-14}$$

P_s is the surface pressure. Although g decreases with altitude, the

*Water vapor gradients contribute less than 1 millimeter above 10° elevation.

effect is small and can be neglected in (2-14). The temperature T is assumed to have a linear slope

$$T = T_s + \beta h \qquad (2\text{-}15)$$

where T_s is the surface temperature and β is the temperature lapse rate. The integration in (2-14) using (2-15) gives

$$P = P_s \left(\frac{T}{T_s}\right)^{-Mg/R\beta} . \qquad (2\text{-}16)$$

The group refractivity is obtained by substituting (2-15) and (2-16) into (2-10) and neglecting the water vapor contribution.

$$N_g = 80.343\ f(\lambda)\ \frac{P_s}{T_s}\left(1 + \frac{\beta h}{T_s}\right)^{-Mg/R\beta} \qquad (2\text{-}17)$$

The horizontal coordinate ρ in (2-9) is also a function of altitude. ρ may be approximated by its value along the straight-line path R_s

$$\rho = r_0 \sin^{-1}\left\{\frac{-\left(\frac{r_0}{r_0 + h}\right) + \left[1 + \frac{1}{\tan^2 E} \cdot \frac{(r_0 + h)^2 - r_0^2}{(r_0 + h)^2}\right]^{1/2}}{\cot E + \tan E}\right\} \qquad (2\text{-}18)$$

where E is the satellite elevation angle. When E is 10° or larger, the integrand in (2-9) is significant only for h less than about 100 km. In this region the square root in the argument of the arc sine can be approximated by the first two terms in the binomial series

$$\rho \approx r_0 \sin^{-1}\left[\frac{h}{r_0 \tan E} - \frac{1}{2}\frac{\cos^2 E}{\tan^3 E}\frac{h^2}{r_0^2}\right] \approx \frac{h}{\tan E}\left(1 - \frac{1}{2}\frac{\cos^2 E}{\tan^2 E}\frac{h}{r_0}\right) . \qquad (2\text{-}19)$$

The term $\frac{h}{\tan E}$ in (2-19) is the value of ρ for a flat earth model. The second term is a correction for the more realistic spherical earth model.

It is significant only at the lower elevation angles.

The altitude dependence of $\frac{1}{\sin\theta_0}$ is determined by solving (2-2) for $\frac{1}{\sin\theta}$ and expanding the result in inverse powers of $\sin\theta_0$ (see Gardner and Rowlett [6]). The two most significant terms are

$$\frac{1}{\sin\theta} \approx \frac{1}{\sin E} - \frac{1}{\sin^3 E}\frac{h}{r_o} \quad . \tag{2-20}$$

Now substituting (2-19) and (2-20) into (2-9) and retaining only first- and second-order terms in ρ, we have

$$GC_1 = \frac{10^{-6}}{\sin E \tan E}\frac{\partial}{\partial\rho'}\left\{\int_0^\infty dh\, N_g(h,\rho')\, h\left[1 - \frac{(1 + 1/2\cos^4 E)}{\sin^2 E}\frac{h}{r_o}\right]\right\}\Bigg|_{\rho'=0} \quad . \tag{2-21}$$

The integrals can now be evaluated by using the expression in (2-17) for N_g

$$GC_1 = \frac{C}{\sin E \tan E}\frac{\partial}{\partial\rho}\left(P_s T_s K_s\right)\Big|_{\rho=0} + \frac{D(1 + 1/2\cos^4 E)}{\sin^3 E \tan E}\frac{\partial}{\partial\rho}\left(\frac{P_s T_s^4 K_s^2}{2 - K_s}\right)\Bigg|_{\rho=0} \tag{2-22}$$

$$C = 80.343\, f(\lambda)\frac{R^2}{(Mg)^2}10^{-6} = 6.915 \times 10^{-2}\, f(\lambda) \quad \text{(m)}$$

$$D = -80.343\, f(\lambda)\frac{2}{r_o}\frac{R^3}{(Mg)^3}10^{-6} = -6.362 \times 10^{-7}\, f(\lambda) \quad \text{(m)}$$

where r_o is taken as the nominal earth radius (6378 km), and g has been set equal to 9.784. The correction term GC_1 is given in meters when the listed values for C and D are used and the derivatives are in units of m^{-1}. The value of K_s depends on the temperature lapse rate β. Marini and Murray [1] derived an empirical expression for K_s by numerically

integrating through atmospheres of the U.S. Standard Atmosphere Supplements (1966) and applying a linear regression fit to the values

$$K_s = 1.163 + 0.00968 \cos 2\theta - 0.00104T_s + 0.00001435P_s \qquad (2\text{-}23)$$

θ = colatitude of laser site

The first term in (2-22) is typically three to four centimeters at 10° elevation while the second term is generally one centimeter or less. At 10° elevation roughly two-thirds of the contribution of the second term arises from the expansion of $\frac{1}{\sin\theta}$ (Eq. (2-20)). The remaining contribution is from the spherical earth correction factor in the expansion of ρ (Eq. (2-19)).

The error introduced by neglecting higher-order terms of GC can be estimated by obtaining a bound on the second term in the series

$$GC_2 = \frac{10^{-6}}{2}\left[\frac{\partial^2}{\partial\rho'^2}\int_0^\infty dh\,\frac{N_g(h,\rho')\rho^2}{\sin\theta}\right]\Bigg|_{\rho'=0}$$

$$= \frac{10^{-6}}{2\sin E\tan^2 E}\left[\frac{\partial^2}{\partial\rho'^2}\int_0^\infty dh\, h^2 N_g(h,\rho')\right]\Bigg|_{\rho'=0}. \qquad (2\text{-}24)$$

This integral can be evaluated by substituting the expression given in (2-17) for N_g

$$GC_2 = \frac{80.343\, f(\lambda)}{\sin E\tan^2 E}\frac{R^3}{(Mg)^3}10^{-6}\frac{\partial^2}{\partial\rho^2}\left(\frac{P_s T_s^2 K_s^2}{2 - K_s}\right)\Bigg|_{\rho=0} \qquad (2\text{-}25)$$

$$GC_2 = \frac{2.029\, f(\lambda)}{\sin E\tan^2 E}\frac{\partial^2}{\partial\rho^2}\left(\frac{P_s T_s^2 K_s^2}{2 - K_s}\right)\Bigg|_{\rho=0}.$$

GC_2 is given in meters when the derivative is in units of m^{-2}

III. CALCULATION OF GC_1

Data used in evaluating GC_1 were obtained from radiosonde balloon releases of Project Haven Hop I [5]. Figure 2 displays the locations of the radiosonde release sites. Most sites are seen to be centered about the Washington, D.C. area and to be displaced 100 to 150 kilometers from one another. The radiosondes were released within a few minutes of each other at various times throughout the night and day during January and February of 1970. The balloons monitored pressure, temperature, and relative humidity periodically during their ascent through the atmosphere.

Equation (2-22) is based on a spherical earth model. Data used in evaluating (2-22) should reflect this modeling, i.e., values of pressure and temperature should be obtained from a spherical surface. The raw radiosonde data violated this modeling in two respects. First, for any given group of release sites, each site was a different altitude above sea level. Second, since each balloon was monitored only periodically, raw data points were arbitrary with respect to altitude and to the other balloons in the group.

These inconsistencies were removed from any group of balloon release sites by selecting the altitude of the highest site as the first altitude at which radiosonde data would be available from all stations. Typically this altitude was 140 meters above sea level. Data from the other balloons in the group were interpolated to this altitude using the interpolation procedures described in [1] and [4] for ray-tracing applications.

Method I Two methods were used to evaluate (2-22), or, more specifically, the derivatives $\frac{\partial}{\partial\rho}(P_s T_s K_s)$ and $\frac{\partial}{\partial\rho}\frac{P_s T_s^2 K_s^2}{2 - K_s}$. Method I approximates the derivatives as

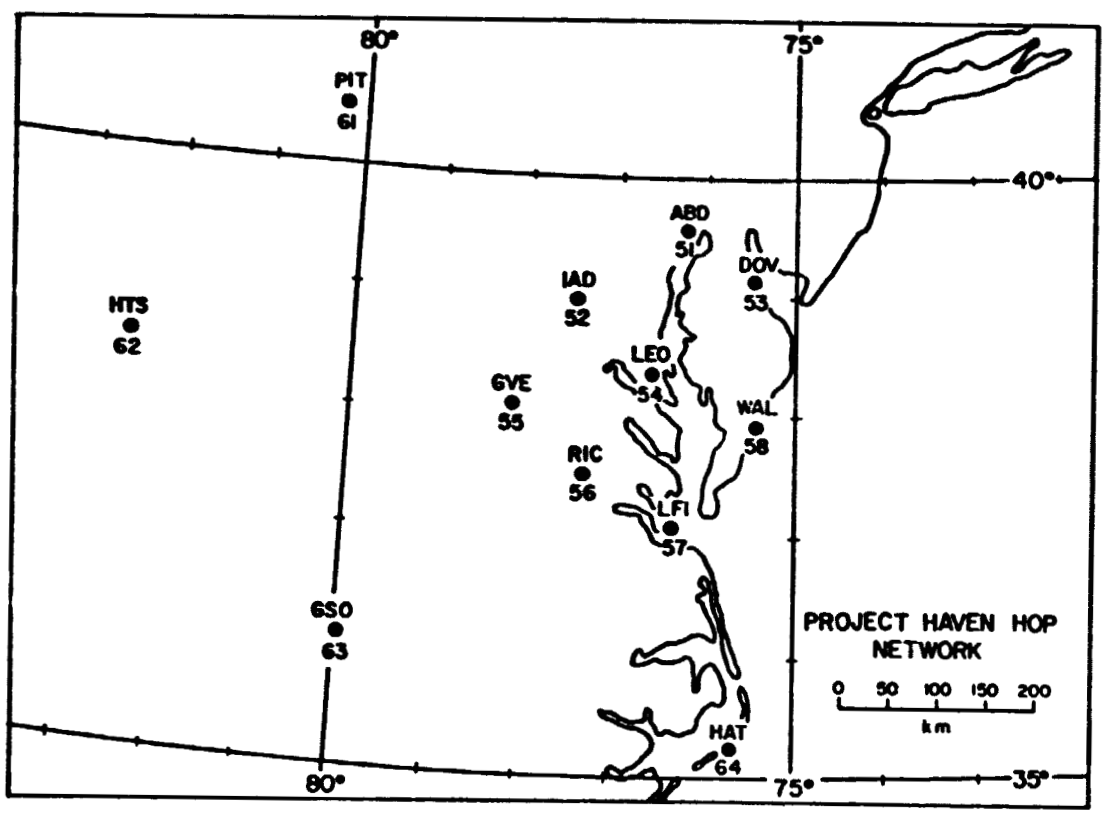

Figure 2. Location of balloon release sites for Project Haven Hop.

$$\frac{\partial}{\partial \rho} (P_s T_s K_s) = \frac{P_1 T_1 K_1 - P_0 T_0 K_0}{\rho_{01}} \tag{3-1}$$

and

$$\frac{\partial}{\partial \rho} \left(\frac{P_s T_s K_s}{2 - K_s} \right) = \left(\frac{P_1 T_1^2 K_1^2}{2 - K_1} - \frac{P_0 T_0^2 K_0^2}{2 - K_0} \right) \frac{1}{\rho_{01}} \tag{3-2}$$

where the subscript 0 indicates the ranging site and the subscript 1 an outlying site located beneath the laser beam trajectory. ρ_{01} is the distance between the two sites (see Fig. 1). The approximate derivatives in (3-1) and (3-2) become more accurate as ρ_{01} approaches zero.

Equations (3-1), (3-2), and thus (2-22) could be evaluated using the raw radiosonde data interpolated to the height of the highest site. For the case where the laser site is located at 54, evaluations of GC_1 would be restricted to azimuths corresponding to those of the peripheral radiosonde sites. In addition the error in GC_1 would be a strong function of the error in any single radiosonde measurement.

These limitations were partially overcome by modeling the interpolated pressure and temperature of a group of sites using a polynomial regression analysis. The interpolated pressure or temperature was chosen as the dependent variable, and colatitude and longitude the independent variables of a multiple regression fit. The regression generated a polynomial giving surface pressure or temperature as a function of location. Note two regressions were performed for each group of sites, one for temperature and another for pressure. In this manner a pressure surface and a temperature surface were created in the vicinity of the laser ranging site at the altitude of the highest site. These surfaces yielded the least squares fit to the interpolated radiosonde data. The polynomial models employed in the regression analysis are given by (3-3) through (3-5)

below

$$M = M_r + \theta \cdot M_\theta + \phi \sin\theta \cdot M_\phi + \theta\phi \sin\theta \cdot M_{\theta\phi} + \theta^2 \cdot M_{\theta\theta} + \phi^2 \sin^2\theta \cdot M_{\phi\phi} \quad (3\text{-}3)$$

$$M = M_r + \theta \cdot M_\theta + \phi \sin\theta \cdot M_\phi + \theta\phi \sin\theta \cdot M_{\theta\phi} \quad (3\text{-}4)$$

$$M = M_r + \theta \cdot M_\theta + \phi \sin\theta \cdot M_\phi \quad (3\text{-}5)$$

where

M = pressure or temperature

$M_r, M_\theta, M_\phi, M_{\theta\phi}, M_{\theta\theta}, M_{\phi\phi}$ = regression coefficients

θ = colatitude = 90° - latitude

ϕ = longitude.

A minimum of six data points is required to determine the regression coefficients in (3-3), four to determine (3-4), and three to determine (3-5).

Range corrections calculated by ray tracing were compared with GC_1 in order to ascertain its usefulness in correcting refraction effects (see Section IV and Gardner and Rowlett [6]). The particular polynomial employed was chosen to be the same as the refractivity model used in performing the ray traces. By using more than the minimum number of stations required to determine a given polynomial the regression served to average out some of the radiosonde errors (see Section VI). Data from eight radiosonde stations were used for quadratic (3-3), or linear (3-5) modeling of pressure and temperature and seven or eight stations for a linear plus cross term model (3-4).

Equations (3-3) through (3-5) allow pressure and temperature to be calculated at any point in the vicinity of the laser ranging site.

Therefore, GC_1 may be calculated at any azimuth or elevation relative to the ranging site. It is also possible to arbitrarily vary ρ_{01}. Because of its central location, site 54 (see Fig. 2) was the ranging site for this investigation.

A typical evaluation of GC_1 proceeds as follows. A model for the pressure and temperature surfaces is selected from (3-3) through (3-5). The data of the appropriate number of stations (7 or 8) are then interpolated to the altitude of the highest station. Two multiple regressions are performed to evaluate regression coefficients which are used to calculate pressure and temperature at the ranging site and at another point a distance ρ_{01} from the ranging site. These values are used to evaluate (3-1) and (3-2) which are then substituted into (2-22) to yield GC_1.

Method II Using Method II the directional derivatives (3-6) and (3-7) are explicitly evaluated at the laser ranging site

$$\left.\frac{\partial}{\partial\rho}\,(P_s T_s K_s)\right|_{\rho=0} \tag{3-6}$$

$$\left.\frac{\partial}{\partial\rho}\left(\frac{P_s T_s^2 K_s^2}{2 - K_s}\right)\right|_{\rho=0} . \tag{3-7}$$

The interpolated radiosonde data were used to calculate the quantities PTK and $[PT^2K^2/(2 - K)]$ at each release station at the altitude of the highest station. These two parameters were then used as the dependent variables of two multiple regressions. The regressions generated polynomials expressing $P_s T_s K_s$ and $\frac{P_s T_s^2 K_s^2}{2 - K_s}$ as a function of location. The modeling of the two quantities was restricted to be linear or quadratic as given by (3-8) and (3-9).

$$F = F_r + \theta \cdot F_\theta + \phi \sin \vartheta \cdot F_\phi \tag{3-8}$$

$$F = F_r + \theta \cdot F_\theta + \phi \sin\theta \cdot F_\phi + \theta\phi \sin\theta \cdot F_{\theta\phi} + \theta^2 \cdot F_{\theta\theta} + \phi^2 \sin^2\theta \cdot F_{\phi\phi} \tag{3-9}$$

where $F_r, F_\theta, F_\phi, F_{\theta\phi}, F_{\theta\theta}, F_{\phi\phi}$ = regression coefficients

$$F = P_s T_s K_s \text{ or } \frac{P_s T_s^2 K_s^2}{2 - K_s} .$$

As in Method I a minimum number of three data points is required to determine the coefficients for model (3-8) and six data points are required for model (3-9). Error averaging in the radiosonde data was achieved by using more than the minimum number of stations in the regressions determining (3-8) and (3-9). Eight data points were used to determine both (3-8) and (3-9). Gradient corrections obtained using Method II were compared with ray traces calculated using quadratic modeling of atmospheric refractivity (see Section IV).

The evaluation of $\frac{\partial F}{\partial \rho}$ is simplified by expressing θ_1 and ϕ_1 as functions of ρ. Note that ρ is the horizontal coordinate measured from the ranging site along the surface of the earth in the direction of the laser beam. Due to the curvature of the earth ρ does not lie in a plane (see Fig. 3). For this reason spherical trigonometry must be used to express θ_1 and ϕ_1 as functions of ρ. The coordinate transformation is given in Appendix II. The results are given in Eqs. (3-10) and (3-11) below.

$$\theta_1 = \cos^{-1}\left[\cos\theta_0 \cos\frac{\rho_{01}}{r_e} + \sin\theta_0 \sin\frac{\rho_{01}}{r_e}\cos\alpha\right] \tag{3-10}$$

$$\phi_1 = \phi_0 + \sin^{-1}\left[\frac{\sin\alpha}{\sin\theta_1}\sin\frac{\rho_{01}}{r_e}\right] \tag{3-11}$$

where

θ_0, ϕ_0 = colatitude and longitude of ranging site

r_e = radius of the earth

α = azimuth of ρ_{01}.

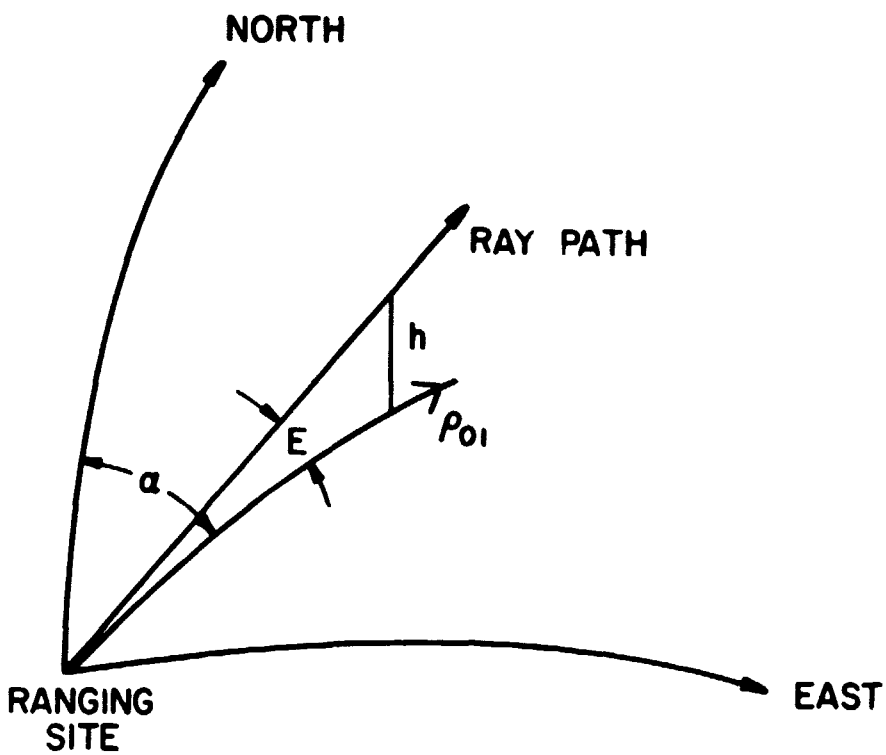

Figure 3. Geometry of ranging site, ray path, and ρ.

Note longitudes west of the prime meridian are taken as negative.

Equations (3-10) and (3-11) may be employed, using the chain rule, to determine $\frac{\partial F}{\partial \rho}$. Separate evaluations of $\frac{\partial F}{\partial \rho}$ are required for the linear model (3-8) and the quadratic model (3-9). Appendix III outlines the steps necessary in this evaluation. The results are given by (3-12) and (3-13).

$$\left.\frac{\partial F}{\partial \rho}\right|_{\rho=0}^{\text{linear}} = \frac{-\cos\alpha}{r_e}\left[F_\theta + \phi_0 \cos\phi_0 \cdot F_\phi\right] + \frac{\sin\alpha}{r_e} \cdot F_\phi \qquad (3\text{-}12)$$

$$\left.\frac{\partial F}{\partial \rho}\right|_{\rho=0}^{\text{quadratic}} = \frac{-\cos\alpha}{r_e}\left[F_\theta + \phi_0 \cos\theta_0 \cdot F_\phi + \phi_0 \sin\theta_0 \cdot F_{\theta\phi} + \phi_0\theta_0 \cos\theta_0 \cdot F_{\theta\phi} + 2\theta_0 \cdot F_{\theta\theta} + \phi_0^2 \sin 2\theta_0 \cdot F_{\phi\phi}\right] + \frac{\sin\alpha}{r_e}\left[F_\phi + \theta_0 \cdot F_{\theta\phi} + 2\phi_0 \sin\theta_0 \cdot F_{\phi\phi}\right] . \qquad (3\text{-}13)$$

To summarize, Method II uses the interpolated radiosonde data from eight stations to calculate regression coefficients for the parameters $P_sT_sK_s$ and $P_sT_s^2K_s^2/(2 - K_s)$. The form of the regression modeling is given by (3-8) or (3-9). The regression coefficients are then substituted into the explicit evaluation of the derivatives $\frac{\partial F}{\partial \rho}$ (evaluated at $\rho = 0$). Equation (3-12) was used for the linear model and (3-13) for the quadratic model. Two evaluations of (3-12) or (3-13) are required; one using the regression coefficients for $P_sT_sK_s$ and another using the regression coefficients for $P_sT_s^2K_s^2/(2 - K_s)$. GC_1 is then calculated by substituting the values of $\left.\frac{\partial P_sT_sK_s}{\partial \rho}\right|_{\rho=0}$ and $\left.\frac{\partial}{\partial \rho}\frac{P_sT_s^2K_s^2}{(2 - K_s)}\right|_{\rho=0}$ into Equation (2-22).

IV. RAY TRACE RANGE CORRECTIONS

The ability of GC_1 to correct laser ranging data for the effects of horizontal refractivity gradients has been investigated. GC_1 was compared with range corrections obtained by ray tracing through three-dimensional refractivity profiles. The profiles were constructed using meteorological data gathered in Project Haven Hop I [5]. The Haven Hop data consist of pressure, temperature and humidity measurements obtained by radiosonde balloons which were released from eleven different locations around the Washington, D.C. area during January and February of 1970. The balloon release sites are indicated on the map in Fig. 2. The balloons were released within a few minutes of each other at various times during the night and day and tracked to an average altitude of 15 km.

At optical frequencies the phase refractivity is given by

$$N = \left[287.604 + \frac{1.6288}{\lambda^2} + \frac{0.0136}{\lambda^4}\right]\left[\frac{P}{1013.25}\right]\left[\frac{273.15}{T}\right] - 11.2683\,\frac{e}{T} \qquad (4\text{-}1)$$

where

λ = laser wavelength (um)

P = atmospheric pressure (mb)

T = atmospheric temperature (°K)

e = water vapor pressure (mb).

The group refractivity can be calculated from (4-1)

$$N_g = N - \lambda\,\frac{dN}{d\lambda} = 80.343 f(\lambda)\,\frac{P}{T} - 11.27\,\frac{e}{T} \qquad (4\text{-}2)$$

where $f(\lambda)$ is given by Eq. (2-12).

Radiosonde observations consist of temperature, pressure, and humidity measurements taken from the surface up to the point where the balloon bursts.

The measurements are obtained at certain standard and significant levels during the balloon ascent. The data can be used in conjunction with Eqs. (4-1) and (4-2) to construct refractivity profiles along the balloon ascent path from the surface up to the point of highest measurement. Above the latter point, the refractivity profile can be extended by assuming a suitable temperature profile. The procedure for constructing the refractivity profiles from the radiosonde data is straightforward and is discussed in detail in Gardner and Rowlett's report [6].

Three-dimensional refractivity profiles can be constructed from the radiosonde profiles by assuming a suitable model for the horizontal refractivity variations. Zanter, Gardner, and Rao [4] used a linear model which required three radiosonde profiles to determine the model parameters. Gardner and Rowlett [6] extended the model to allow for quadratic variations in the horizontal direction. In the present case the refractivity at any point can be written in the form

$$N(\underline{r}) = N_r(h) + \theta \cdot N_\theta(h) + \phi \sin\theta \cdot N_\phi(h) + \theta\phi \sin\theta \cdot N_{\theta\phi}(h) + \theta^2 \cdot N_{\theta\theta}(h) + \phi^2 \sin^2\theta \cdot N_{\phi\phi}(h) \qquad (4\text{-}3)$$

where h is the altitude and θ and ϕ are the colatitude and longitude of the vector $\underline{r} = (h,\theta,\phi)$. θ is proportional to horizontal displacement in the north-south direction and $\phi \sin\theta$ is proportional to horizontal displacement in the east-west direction. The six coefficients N_r, N_θ, N_ϕ, $N_{\theta\phi}$, $N_{\theta\theta}$, and $N_{\phi\phi}$ are constant with respect to θ and ϕ but can change with altitude.

If the refractivity is known at six or more points, the coefficients for any altitude can be calculated using multiple regression. Equipment failures and balloon malfunctions limited the amount of acceptable

radiosonde data to thirty-one releases involving groups of seven or eight balloons per release. When eight radiosonde profiles were available the quadratic model in (4-3) was employed. To reduce the error in the regression coefficients, a four-coefficient model was employed when only seven radiosonde profiles were available.

$$N(\underline{r}) = N_r(h) + \theta \cdot N_\theta(h) + \phi \sin\theta \cdot N_\phi(h) + \theta\phi \sin\theta \cdot N_{\theta\phi}(h) \quad . \quad (4\text{-}4)$$

The phase and group refractivity at any point (h,θ,ϕ) can be computed from the radiosonde data using Eqs. (4-1)-(4-4). The pressure, temperature and humidity measured by each radiosonde are used to construct continuous profiles of group and phase refractivity along seven or eight balloon ascent paths using (4-1) and (4-2). The coefficients for the models in (4-3) and (4-4) are calculated from these profiles using multiple regression. The coefficients are substituted into (4-3) and (4-4) to obtain the three-dimensional refractivity profiles which can then be employed in the ray-tracing programs.

Range corrections were computed by ray tracing through the three-dimensional refractivity profiles. These corrections are denoted by RT_3. RT_3 is dependent on azimuth since the refractivity is assumed to vary in the horizontal direction. Therefore, azimuth was varied from 0° to 360° in 10° increments. Ray-trace corrections were calculated for each set of radiosonde data at 10°, 20°, 40° and 80° elevation. The laser tracking station was assumed to be located at site 54 in Leonardstown, Md. (Fig. 2). An additional range correction, RT_1, was also computed by ray tracing through a suitable spherically symmetric profile constructed from radiosonde data. RT_3 includes the effects of horizontal gradients, while RT_1 contains no gradient effects. The difference between RT_3 and RT_1

is the range error contributed by the horizontal refractivity gradients.

Complete details of the ray-tracing procedure are available in reference [6].

V. COMPARISON OF GC_1 WITH RANGE CORRECTIONS DERIVED FROM RAY TRACING

A total of 31 sets of data were processed to determine the accuracy with which GC_1 corrected for atmospheric refractivity gradients. Each set employed the meteorological data from a release of eight radiosonde balloons to calculate GC_1 and perform ray traces. Ray-trace correction terms were calculated for each set at 10° increments in azimuth and elevations of 10, 20, 40 and 80 degrees. RT_3 is the range correction obtained by ray tracing through three-dimensional refractivity profiles. It contains the effects of horizontal gradients and depends on both azimuth and elevation. RT_1 is the range correction obtained by ray tracing through spherically symmetric refractivity profiles. The gradient effects in the ranging data are isolated by calculating the term $RT_3 - RT_1$. Any effects not compensated for by GC_1 are given by the error term $\Delta = (RT_3 - RT_1) - GC_1$.

A value of GC_1 was calculated for comparison with each ray trace using each of the methods outlined in Section III. They are briefly summarized as follows:

MODEL a: Use Method I to approximate the derivatives (3-1) and (3-2) and use a quadratic model (3-3) for the surface pressure and temperature.

MODEL b: Use Method I and employ a four-coefficient (3-4) model for the surface pressure and temperature.

MODEL c: Use Method II to evaluate the derivatives (3-12) and (3-13) and use a linear model for $P_s T_s K_s$ and $\frac{P_s T_s^2 K_s^2}{2 - K_s}$.

MODEL d: Use Method II and employ a quadratic model for $P_s T_s K_s$ and $\frac{P_s T_s^2 K_s^2}{2 - K_s}$.

The 31 data sets may be divided into three groups. Group A consisted of 21 sets of data evaluated using modeling scheme a. Group B consisted of 10 arbitrarily selected sets from Group A which were reevaluated using the remaining modeling schemes b, c, and d. Group C* consisted of 10 sets of data evaluated using modeling scheme b. The groups and models are summarized in Appendix VI.

Thirty-six range corrections, RT_3 (one for every 10° increment in azimuth), were calculated for each data set at each elevation angle. A single value of RT_1 was obtained for each data set at each elevation. Therefore there were 756 values of the uncorrected gradient error $RT_3 - RT_1$ calculated for Group A at each elevation angle. Similarly, 360 values of $RT_3 - RT_1$ were calculated for Groups B and C at each elevation angle. Table 1 gives the mean and standard deviation of $RT_3 - RT_1$ for each group. The values of RT_3 used in these calculations employed quadratic refractivity models for groups A and B. Group C employed a four-coefficient refractivity model. In addition, group B was reprocessed using a four-coefficient refractivity model and given the designation Bb in agreement with the labeling scheme for GC$_1$.

TABLE I.

$RT_3 - RT_1$ UNCORRECTED GRADIENT ERROR (cm)

Elevation	10°		20°		40°		80°	
Group	Std	Mean	Std	Mean	Std	Mean	Std	Mean
A	1.96	.01	.51	.00	.12	.00	.01	.00
B	1.90	-.10	.50	-.01	.12	.00	.01	.00
Bb	1.76	-.22	.46	-.03	.11	.00	.01	.00
C	1.90	-.01	.29	.01	.11	.00	.01	.00

*Group A, B and Bb ray traces were obtained using eight radiosonde profiles. Group C ray traces were obtained using seven radiosonde profiles.

Tables 2 through 5 give the mean and standard deviation of the residual error $\Delta = (RT_3 - RT_1) - GC_1$ for all groups and models. Comparison of Table 1 with Tables 2 through 5 indicates the standard deviation of the uncorrected gradient error has been reduced by almost or -half.

TABLE 2.

ERROR AFTER CORRECTION Δ (cm) $E = 10° \pm$

	GROUP A		GROUP B		GROUP C	
	Std	Mean	Std	Mean	Std	Mean
Model a	1.19	.06	1.17	-.03		
Model b			1.13	.01	1.41	-.22
Model c			1.30	-.09		
Model d			1.16	-.10		

TABLE 3.

ERROR AFTER CORRECTION Δ (cm) $E = 20° \pm$

	GROUP A		GROUP B		GROUP C	
	Std	Mean	Std	Mean	Std	Mean
Model a	.31	.02	.31	.01		
Model b			.30	.01	.37	-.03
Model c			.31	-.01		
Model d			.31	-.01		

TABLE 4.

ERROR AFTER CORRECTION Δ (cm) E = 40° ++

	GROUP A		GROUP B		GROUP C	
	Std	Mean	Std	Mean	Std	Mean
Model a	.07	.04	.07	.00		
Model b			.07	.00	.09	-.00
Model c			.07	.00		
Model d			.07	.00		

TABLE 5.

ERROR AFTER CORRECTION Δ (cm) E = 80° ++

	GROUP A		GROUP B		GROUP C	
	Std	Mean	Std	Mean	Std	Mean
Model a	.01	.00	.01	.00		
Model b			.01	.00	.01	.00
Model c			.01	.00		
Model d			.01	.00		

++Results given for models a and b use a separation distance ρ_{01} = 25 km. Group/Model Bc was compared with $RT_3 - RT_1$, calculated using a quadratic refractivity profile for RT_3.

The mean and standard deviation of $RT_3 - RT_1$ and Δ were computed for each azimuth and elevation angle. The results for Group/Model Aa are plotted in Figs. 4 through 11. GC_1 effectively removes the large biases in $RT_3 - RT_1$ at each azimuth. However, the reduction in the mean uncorrected error $(\overline{RT_3 - RT_1})$ has been accompanied by an increase in the standard deviation of the error after correction. We believe the increase

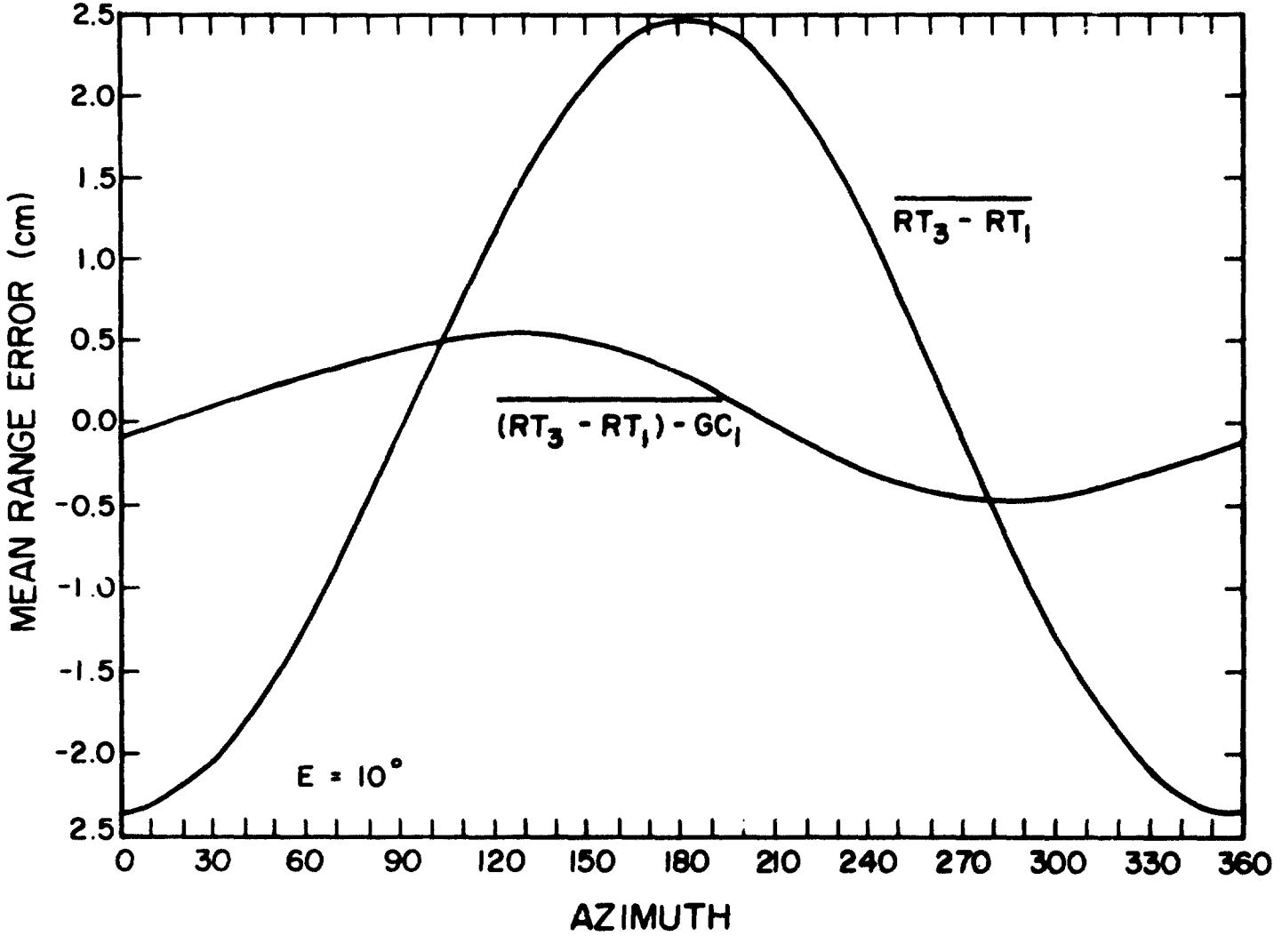

Figure 4. Mean of $RT_3 - RT_1$ and $(RT_3 - RT_1) - GC_1$ versus azimuth. Elevation 10°. Twenty-one data sets comprising Group A. Processed using Model a (see page 78)

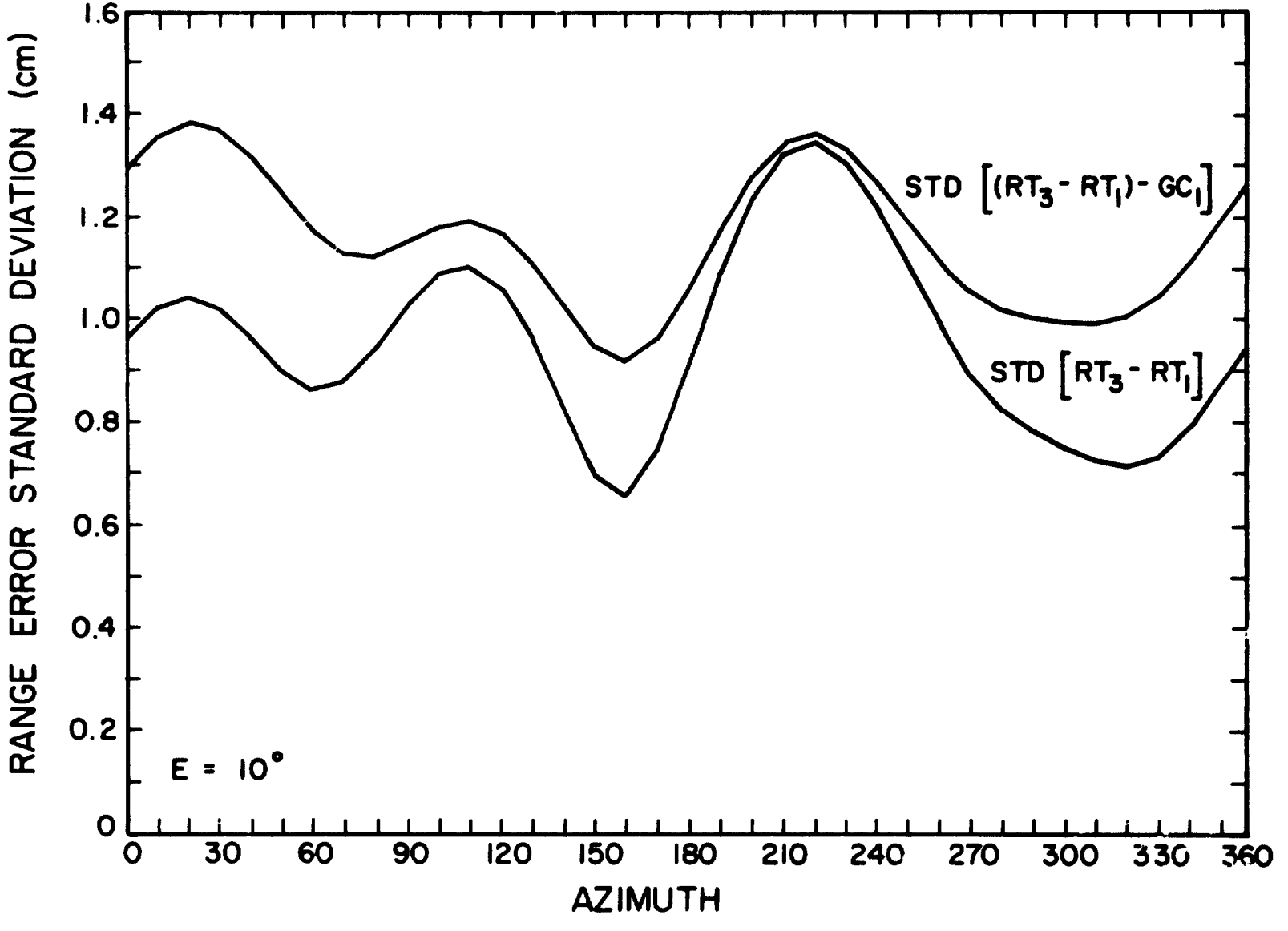

Figure 5. Standard deviation of $RT_3 - RT_1$ and $(RT_3 - RT_1) - GC_1$ versus azimuth. Elevation 10°. Twenty-one data sets comprising Group A. Processed using Model a (see page 78)

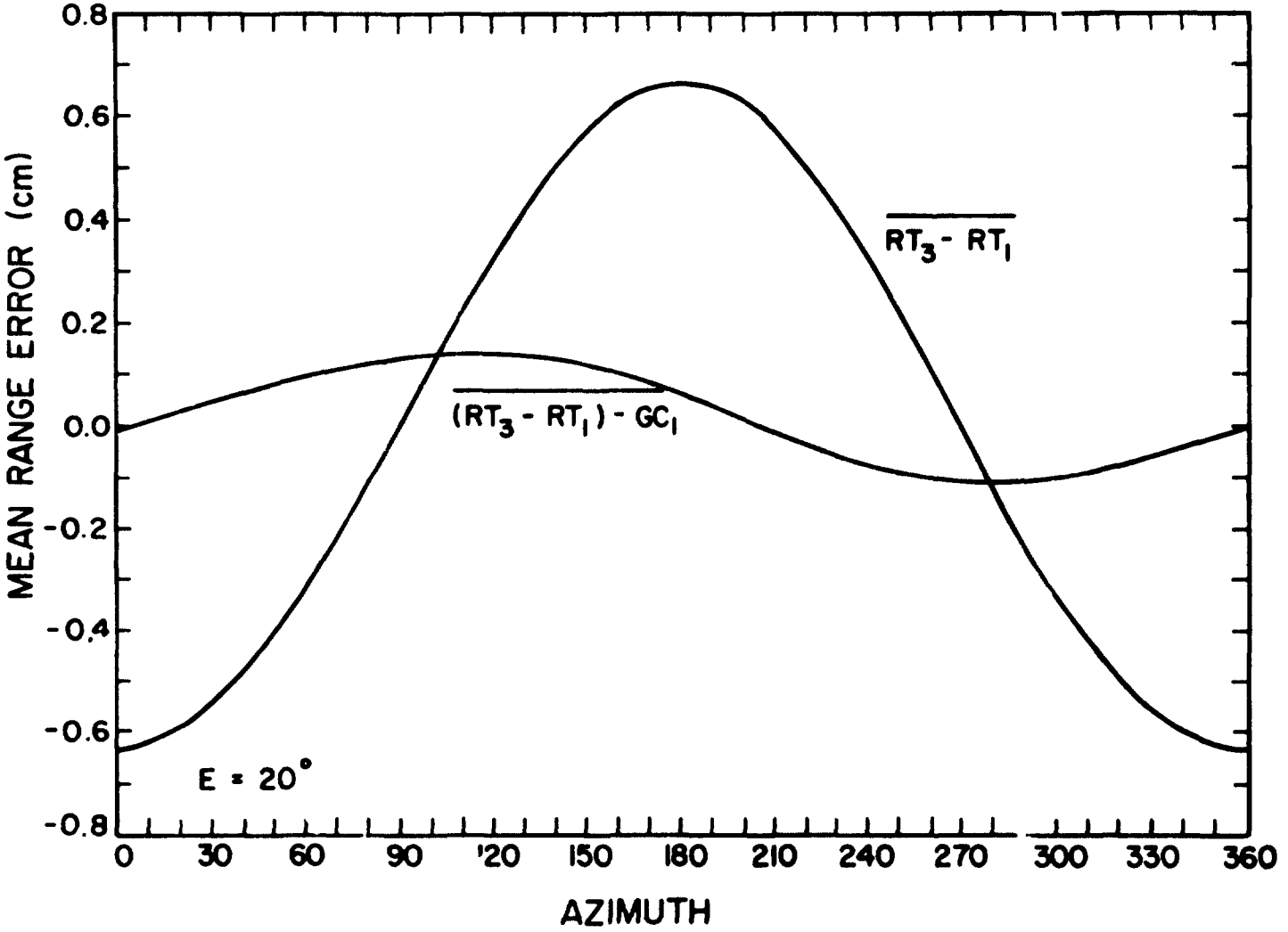

Figure 6. Mean of $RT_3 - RT_1$ and $(RT_3 - RT_1) - GC_1$ versus azimuth. Elevation 20°. Twenty-one data sets comprising Group A. Processed using Model a (see page 78)

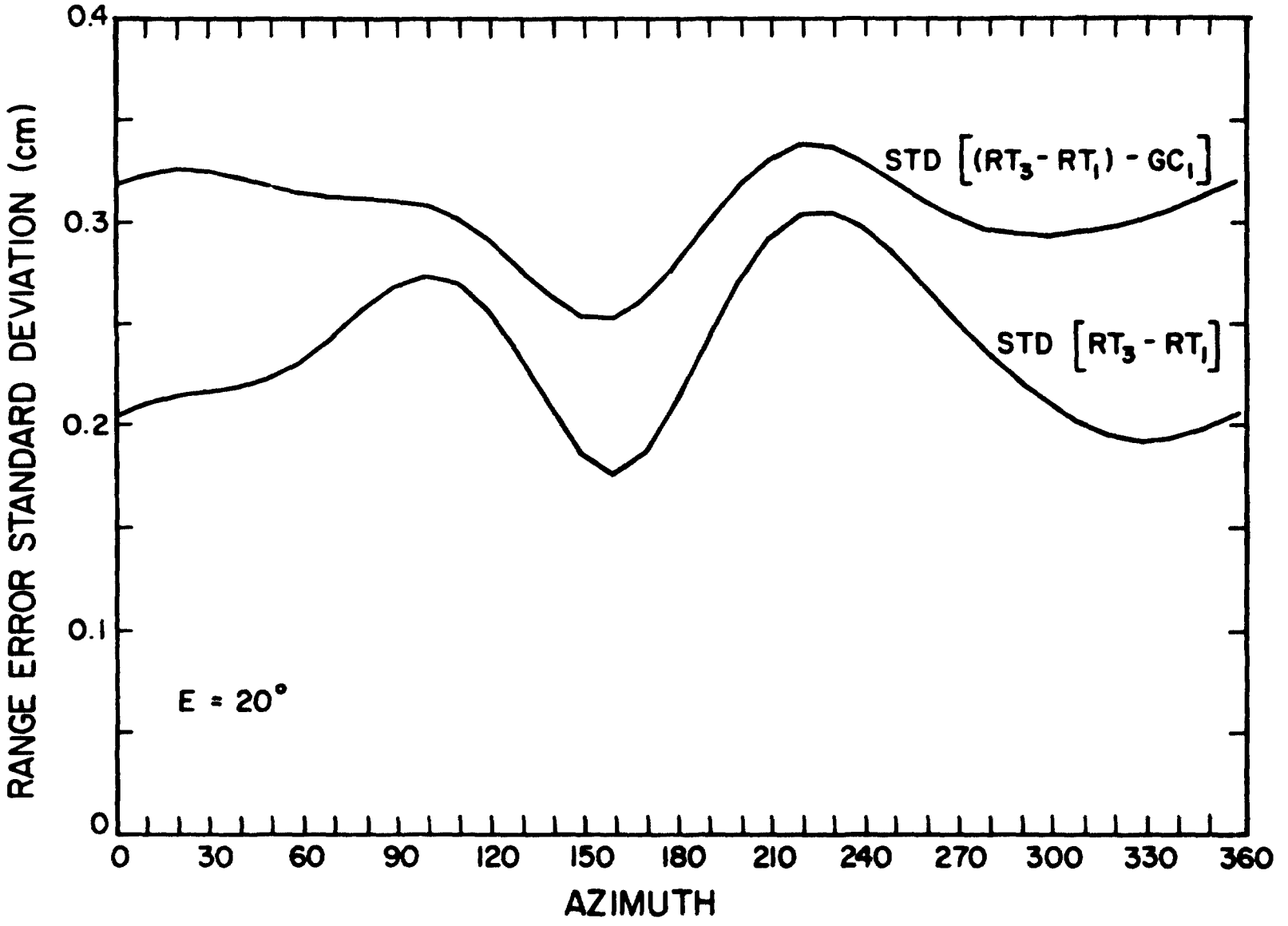

Figure 7. Standard deviation of $RT_3 - RT_1$ and $(RT_3 - RT_1) - GC_1$ versus azimuth. Elevation 20°. Twenty-one data sets comprising Group A. Processed using Model a (see page 78)

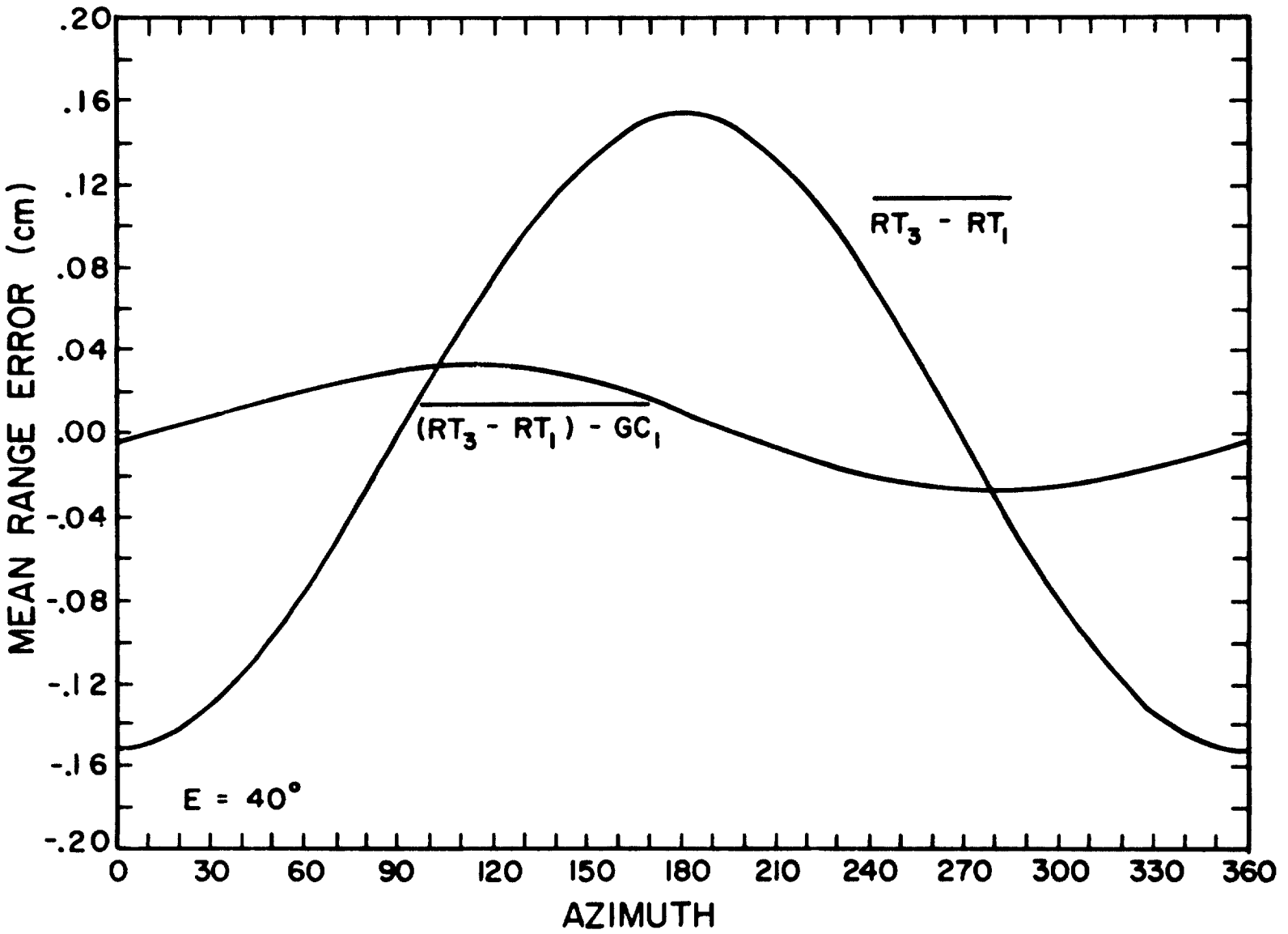

Figure 8. Mean of $RT_3 - RT_1$ and $(RT_3 - RT_1) - GC_1$ versus azimuth. Elevation 40°. Twenty-one data sets comprising Group A. Processed using Model a (see page 78)

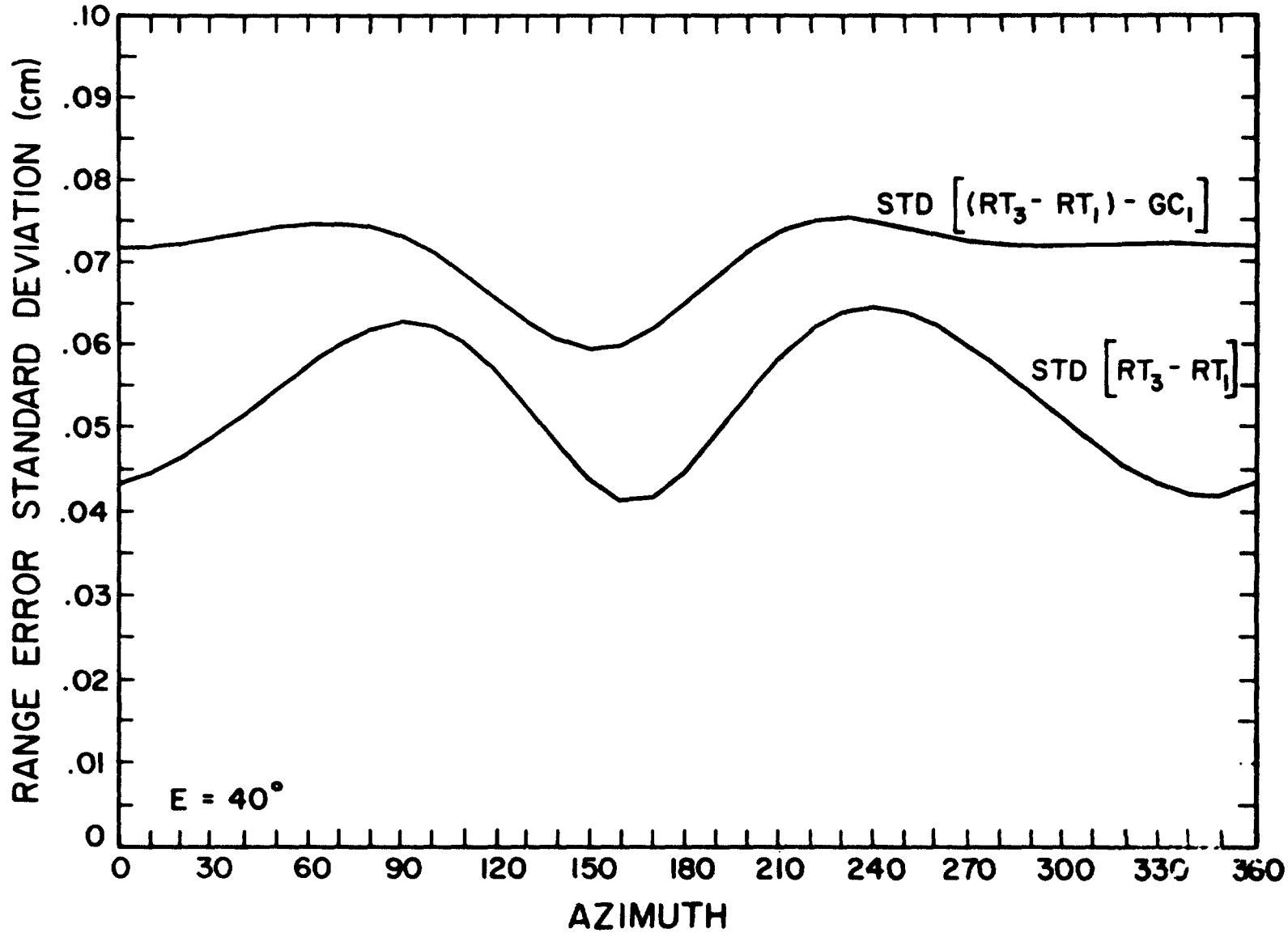

Figure 9. Standard deviation of $RT_3 - RT_1$ and $(RT_3 - RT_1) - GC_1$ versus azimuth. Elevation 40°. Twenty-one data sets comprising Group A. Processed using Model a (see page 78)

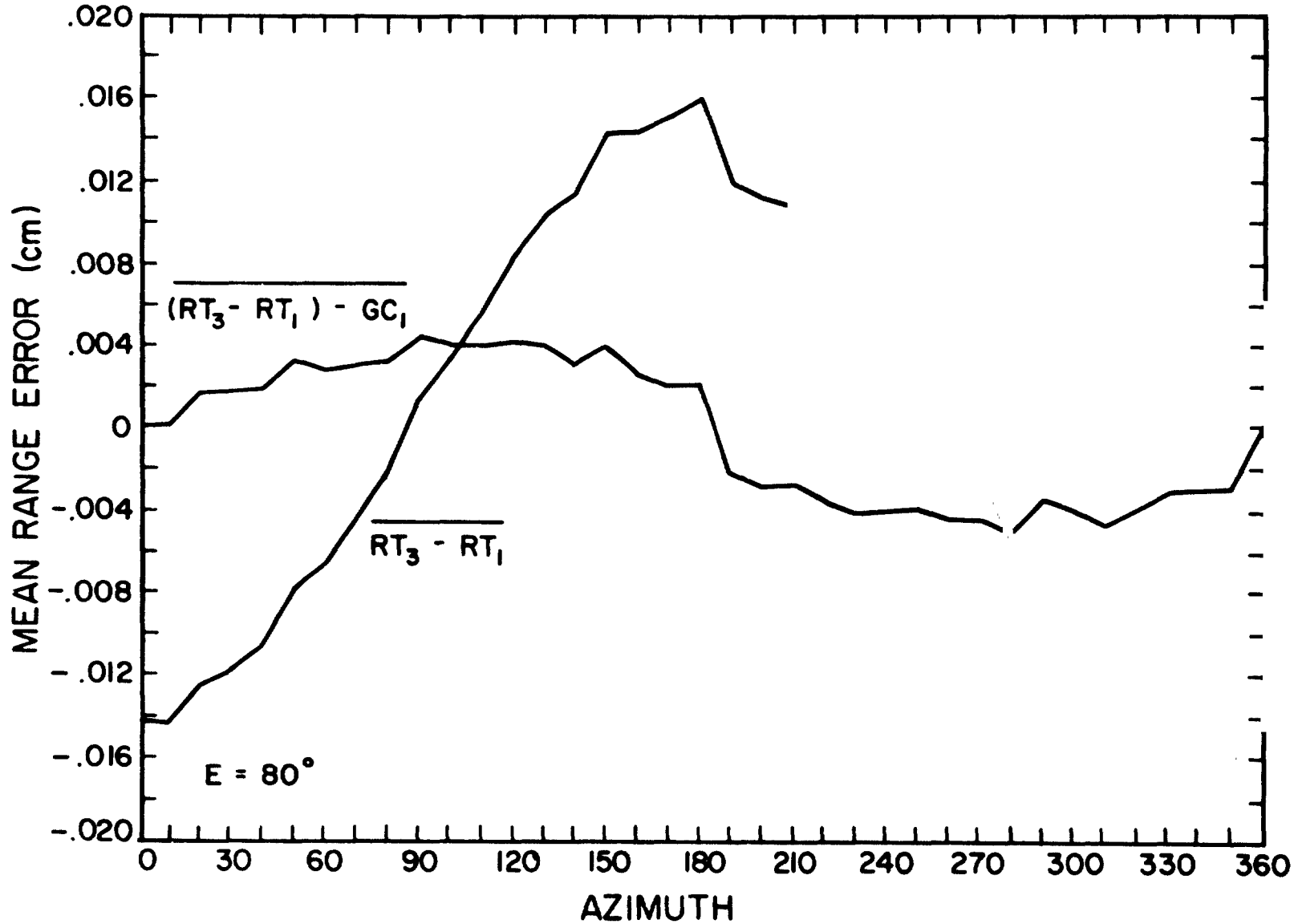

Figure 10. Mean of $RT_3 - RT_1$ and $(RT_3 - RT_1) - GC_1$ versus azimuth. Elevation 80°. Twenty-one data sets comprising Group A. Processed using Model a (see page 78)

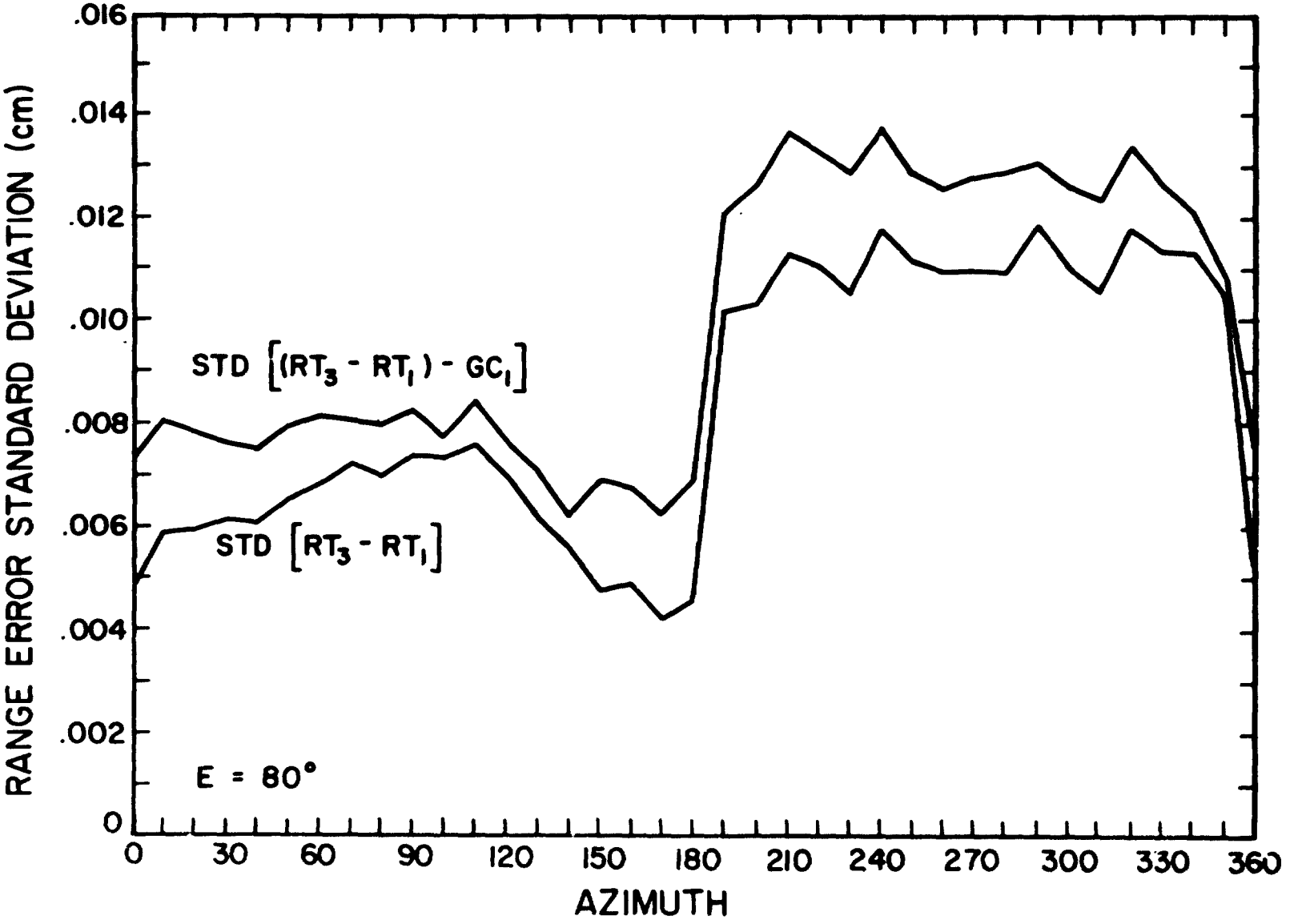

Figure 11. Standard deviation of $RT_3 - RT_1$ and $(RT_3 - RT_1) - GC_1$ versus azimuth. Elevation 80°. Twenty-one data sets comprising Group A. Processed using Model a (see page 78)

can be attributed to measurement errors in the radiosonde data which are used to calculate GC_1 (see Section VI). The E = 80° curve shows the effects of computer round-off noise in the ray-trace routine (see Gardner and Rowlett [6]).

In evaluating GC_1, Method I uses (3-1) and (3-2) to approximate the derivatives. The accuracy of this approximation would be expected to improve as ρ_{01} becomes small. The effect of varying ρ_{01} is shown in Figs. 12 and 13, where corrections using Group/Models Aa, Ba, Bb and Cb are compared. Values of Δ for these groups were calculated for 10° increments in azimuth and separations ρ_{01} = 25, 50, 100, 150, 200 and 300 kilometers. The elevation angle is 10°. For each ρ_{01} the mean and standard deviation of Δ was calculated and plotted as shown. The plots converge for Aa, Ba and Bb at $\rho_{01} \approx 25$ km. If we examine the results in Tables 2 through 5, and compare Models c and d with Models a and b (results for ρ_{01} = 25 km are given in the tables), we see Methods I and II give approximately the same residual errors for small ρ_{01}.

Group/Model Cb has a higher mean and standard deviation than the other groups. Recall the radiosonde releases in Group C contained only seven balloons per release while A and B contained eight. This degradation in the magnitude of the residuals, Δ, can be attributed to the reduction in the number of monitoring stations (see Section VI). The flatness of the curves employing the four-coefficient model is due to the inherent linearity of the model itself. Regardless of the two points we select on a linearly modeled $P_s T_s K_s$ surface, the gradient or slope will always be a constant. Therefore we would not expect GC_1 to vary with ρ_{01} under this modeling scheme.

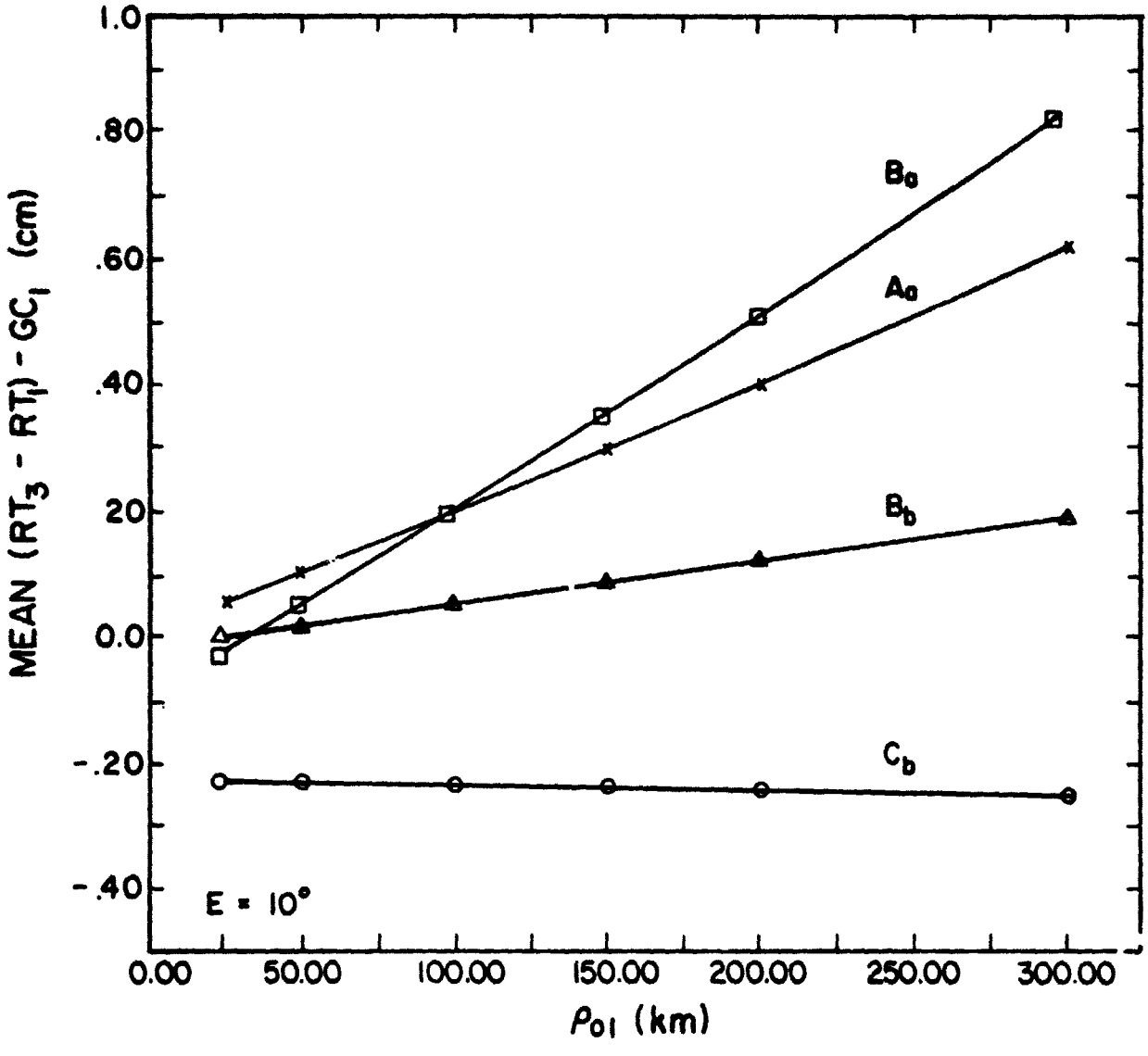

Figure 12. Mean residual error $(RT_3 - RT_1) - GC_1$ versus ρ_{o1} for Group/Models Aa, Ba, Bb, Cb. Group A consists of 21 data sets. Group B consists of 10 arbitrarily selected data sets of Group A. Groups A and B employ radiosonde releases consisting of 8 balloons. Group C consists of 10 data sets employing 7 radiosonde balloons. Models are explained on page 78.

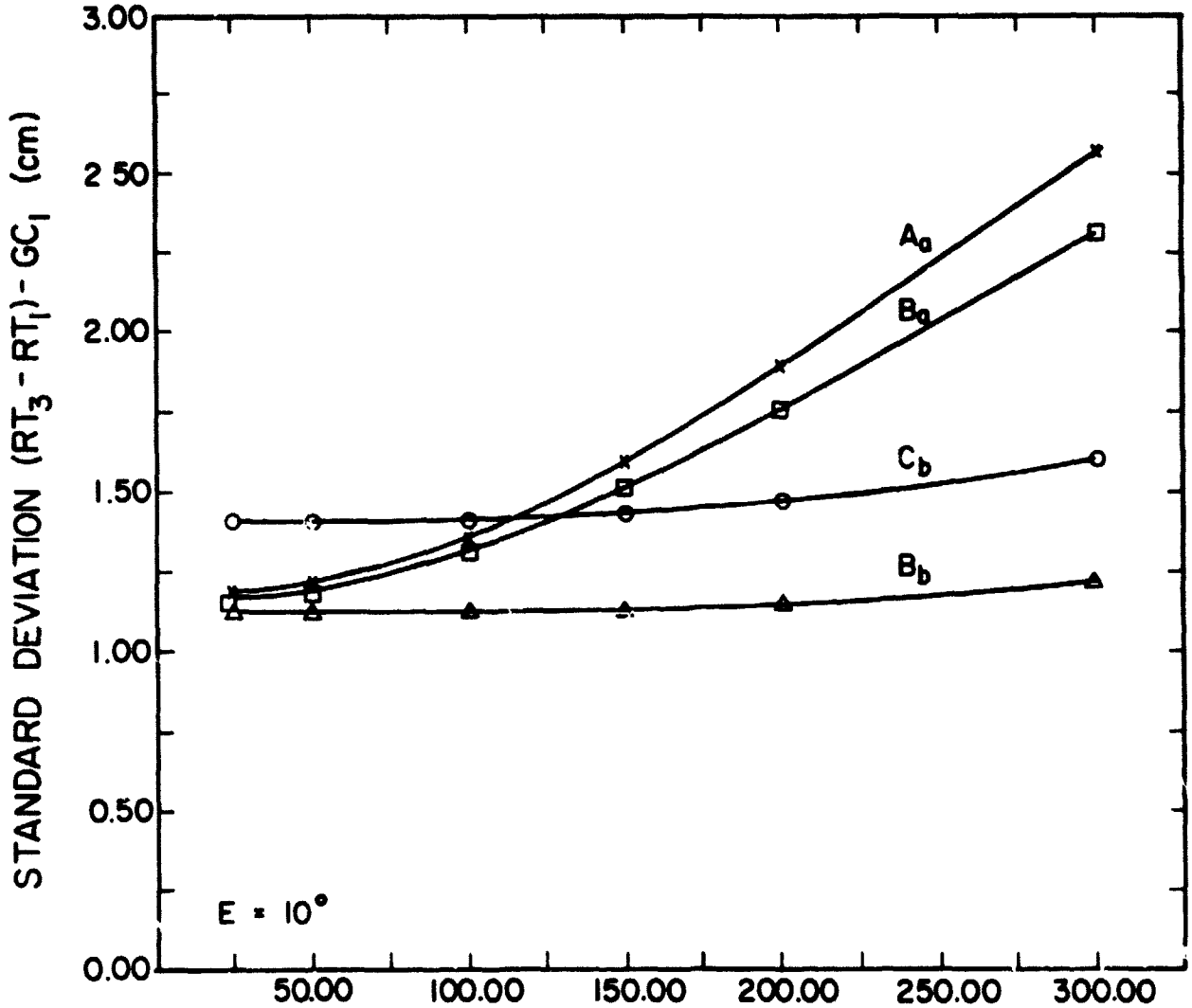

Figure 13. Standard deviation of the residual error $(RT_3 - RT_1) - GC_1$ versus ρ_{01} for Group/Models Aa, Ba, Bb, Cb. Group A consists of 21 data sets. Group B consists of 10 arbitrarily selected data sets of Group A. Groups A and B employ radiosonde releases consisting of 8 balloons. Group C consists of 10 data sets employing 7 radiosonde balloons. Models are explained on page 78.

A typical correction of two data sets from Group/Model Bd is shown in Figs. 14 and 15 where we have plotted $RT_3 - RT_1$ and Δ versus azimuth. Figure 14 shows data of 1530 2/16/70 elevation 10°. GC_1 was fairly effective in reducing the gradient errors $RT_3 - RT_1$. The mean and standard deviations of the 36 residual errors Δ are -.34 and .34 centimeters, respectively. Figure 15 shows data of 1730 2/16/70. GC_1 was not as effective in this data set. The mean and standard deviation of the 36 Δ's at 10° elevation are .25 and .84 centimeters, respectively.

Figures 16 through 19 are histograms of $RT_3 - RT_1$ and Δ for the 21 sets of data processed using Group/Model Aa. Elevations are 10 and 20 degrees. Peak gradient errors are seen to be reduced through the addition of GC_1. Figure 20 gives the percentage of the uncorrected errors, $RT_3 - RT_1$, and the errors after correction, Δ, less than the abscissa value for E = 10° and Group/Model Aa. Approximately 78 percent of the errors before correction were less than ±1 cm. After correction approximately 53 percent of the residual errors were less than ±1 cm.

It is important to note that, regardless of the method used to evaluate GC_1, the mean and standard deviation of the residual errors Δ are comparable. Improvements in Δ are obtained by varying ρ and the number of outlying meteorological stations. These factors must be considered in establishing a ranging facility of a given accuracy. Section VI considers the effects of varying the number of stations and errors in the radiosonde data on the standard deviation of Δ.

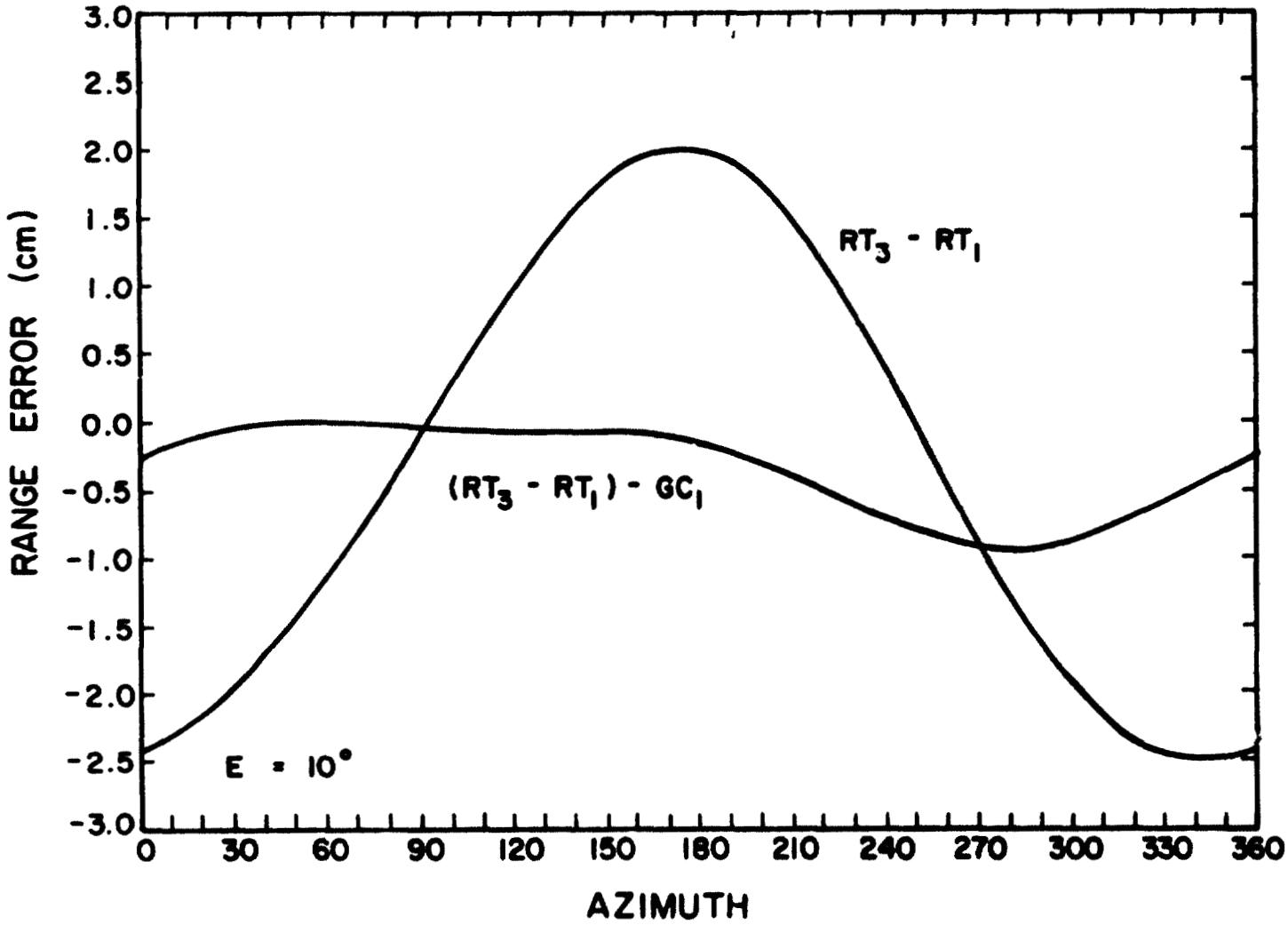

Figure 14. Typical correction of gradient errors $RT_3 - RT_1$ and residual errors $(RT_3 - RT_1) - GC_1$ versus azimuth. Data of 2/16/70 1530 (from Group B) processed using Model d (see page 78). Elevation 10°.

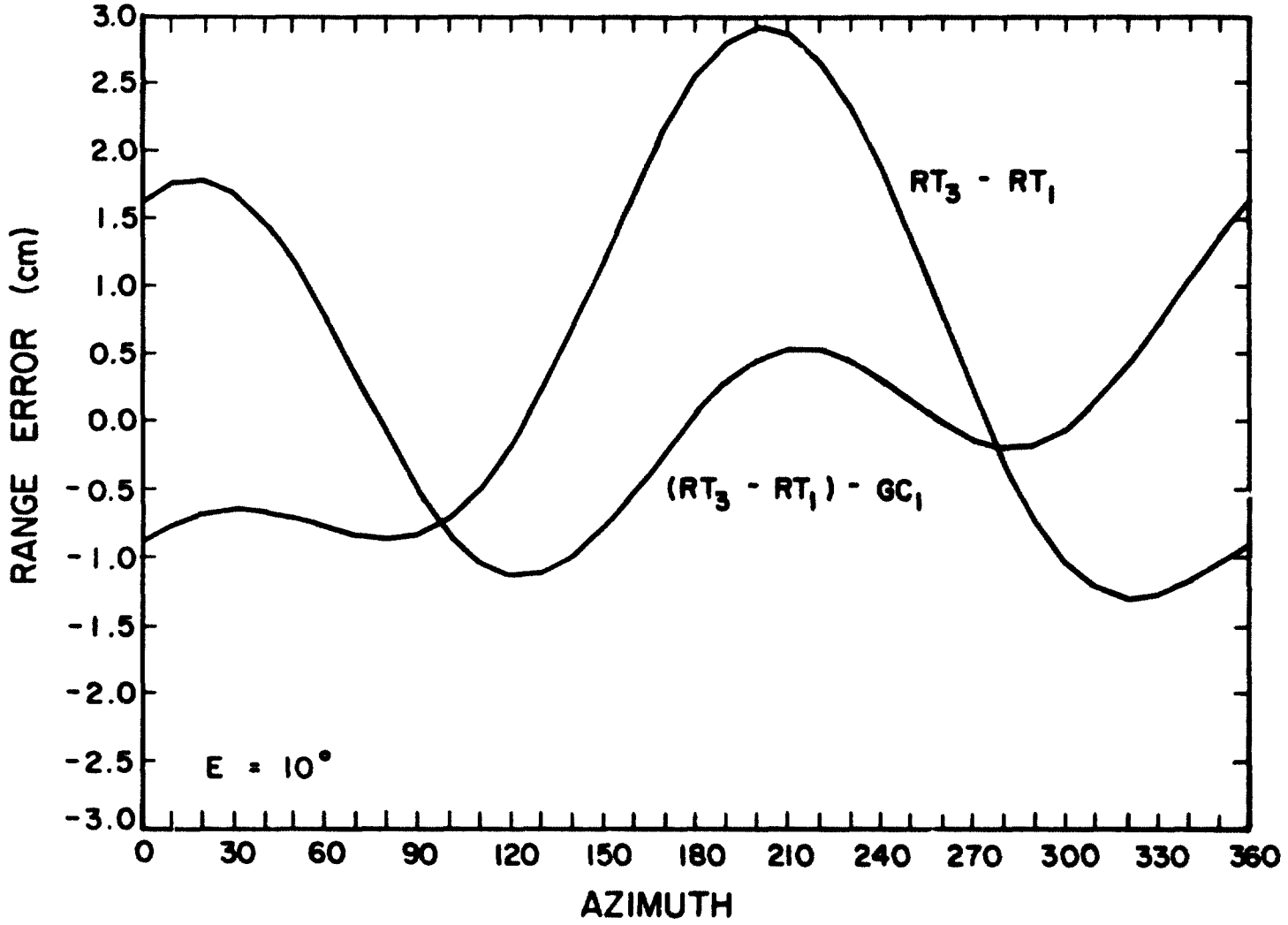

Figure 15. Typical correction of gradient errors $RT_3 - RT_1$ and residual errors $(RT_3 - RT_1) - GC_1$ versus azimuth. Data of 2/16/70 1730 (from Group B) processed using Model d (See page 78). Elevation 10°.

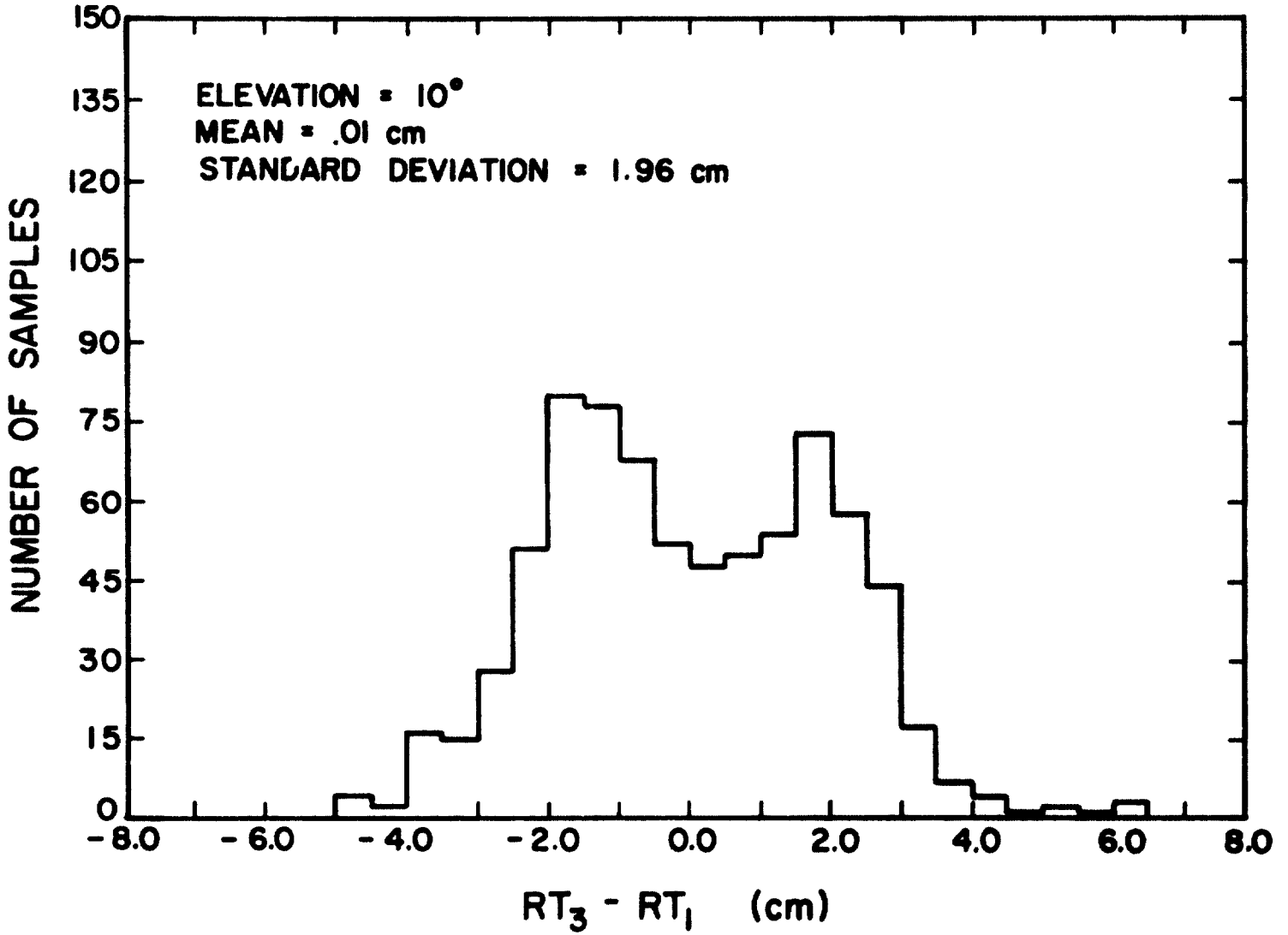

Figure 16. Histogram of uncorrected errors $RT_3 - RT_1$. Elevation = 10°. Twenty-one data sets comprising Group A processed using Model a. Mean = .01 cm. Standard deviation = 1.96 cm.

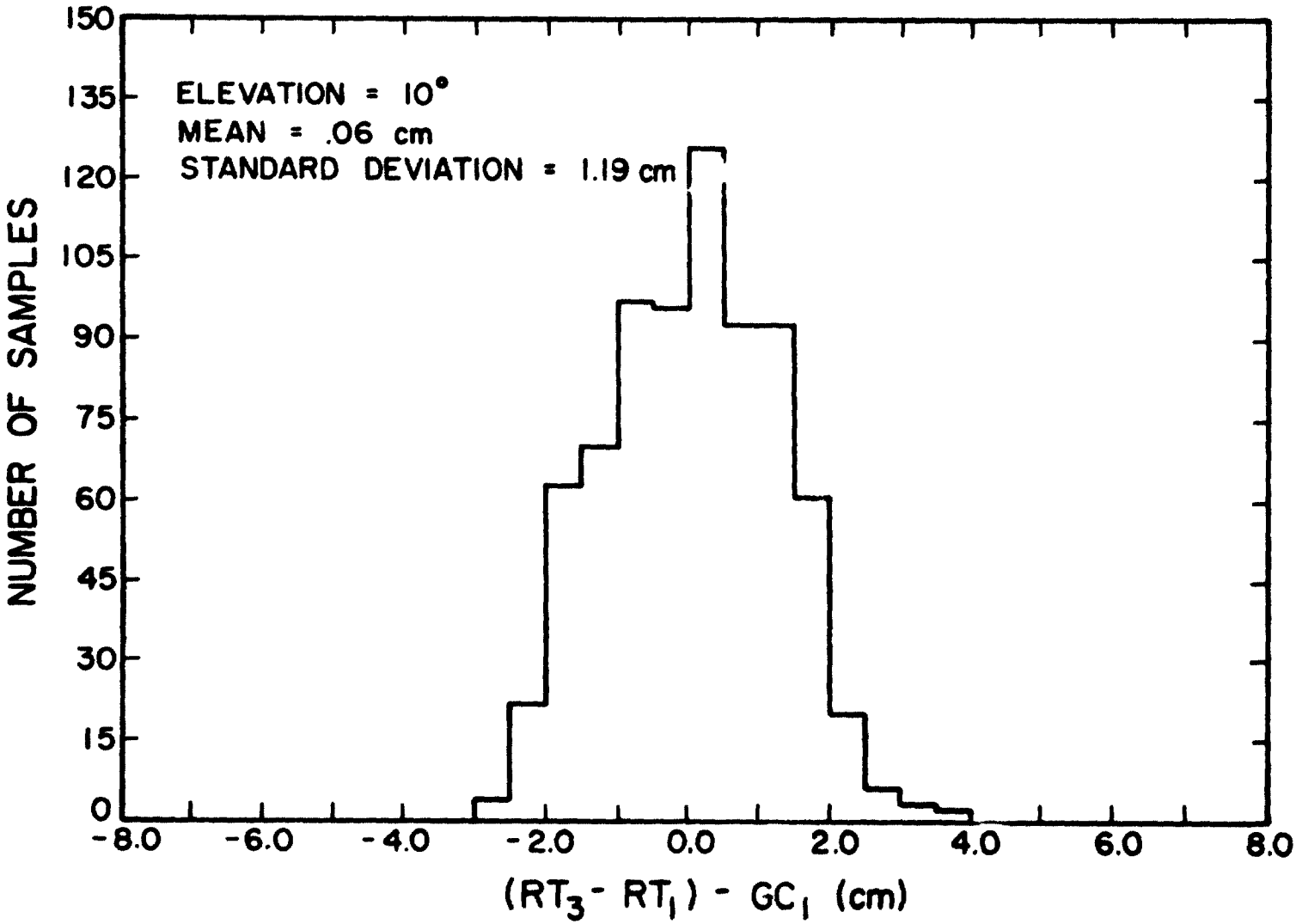

Figure 17. Histogram of residual gradient errors $(RT_3 - RT_1) - GC_1$. Elevation = 10°. Twenty-one data sets comprising Group A processed using Model a. Mean = .06 cm. Standard deviation = 1.19 cm.

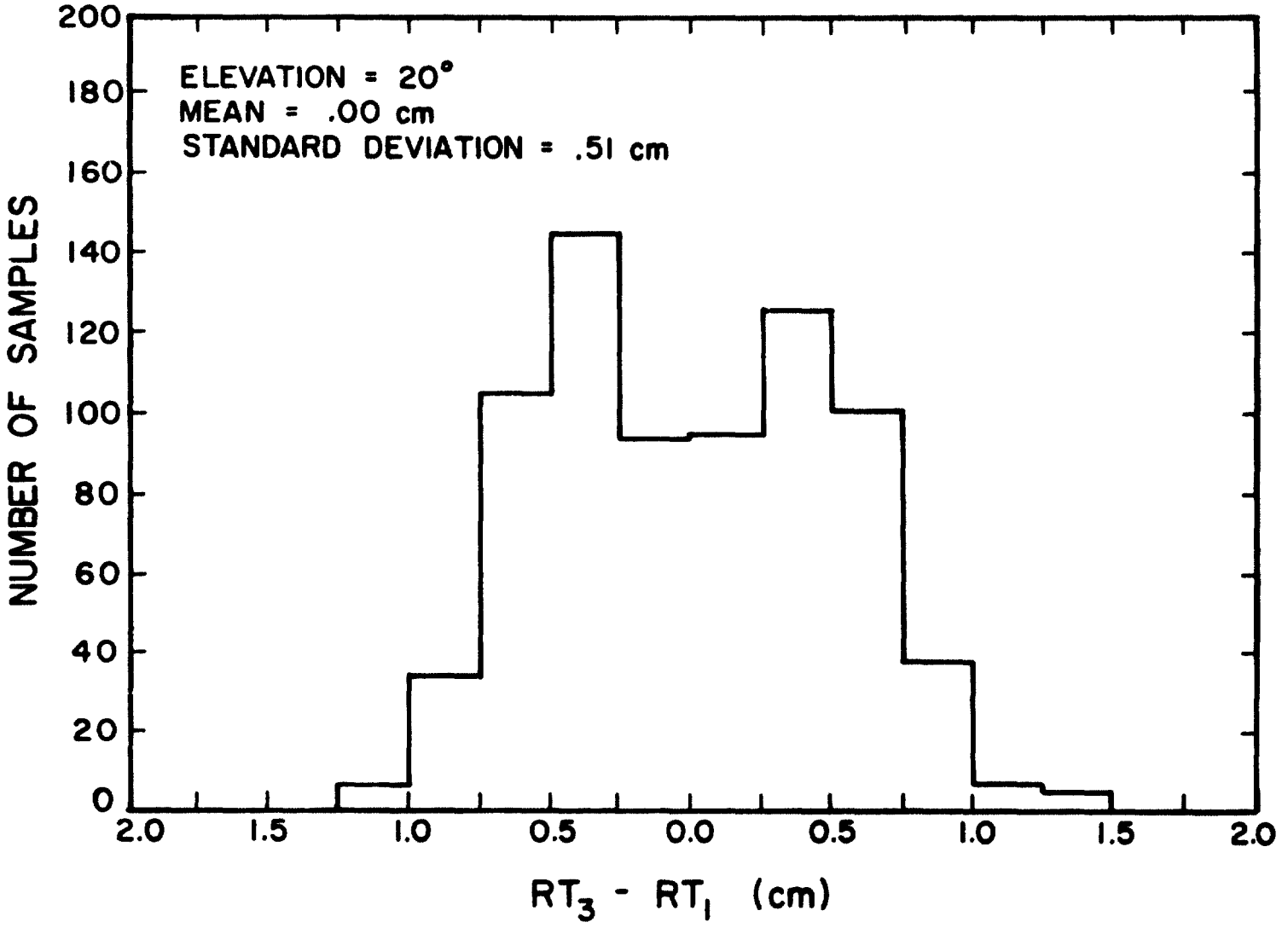

Figure 18. Histogram of uncorrected gradient errors $RT_3 - RT_1$. Elevation = 20°. Twenty-one data sets comprising Group A processed using Model a. Mean = .00 cm. Standard deviation = .51 cm.

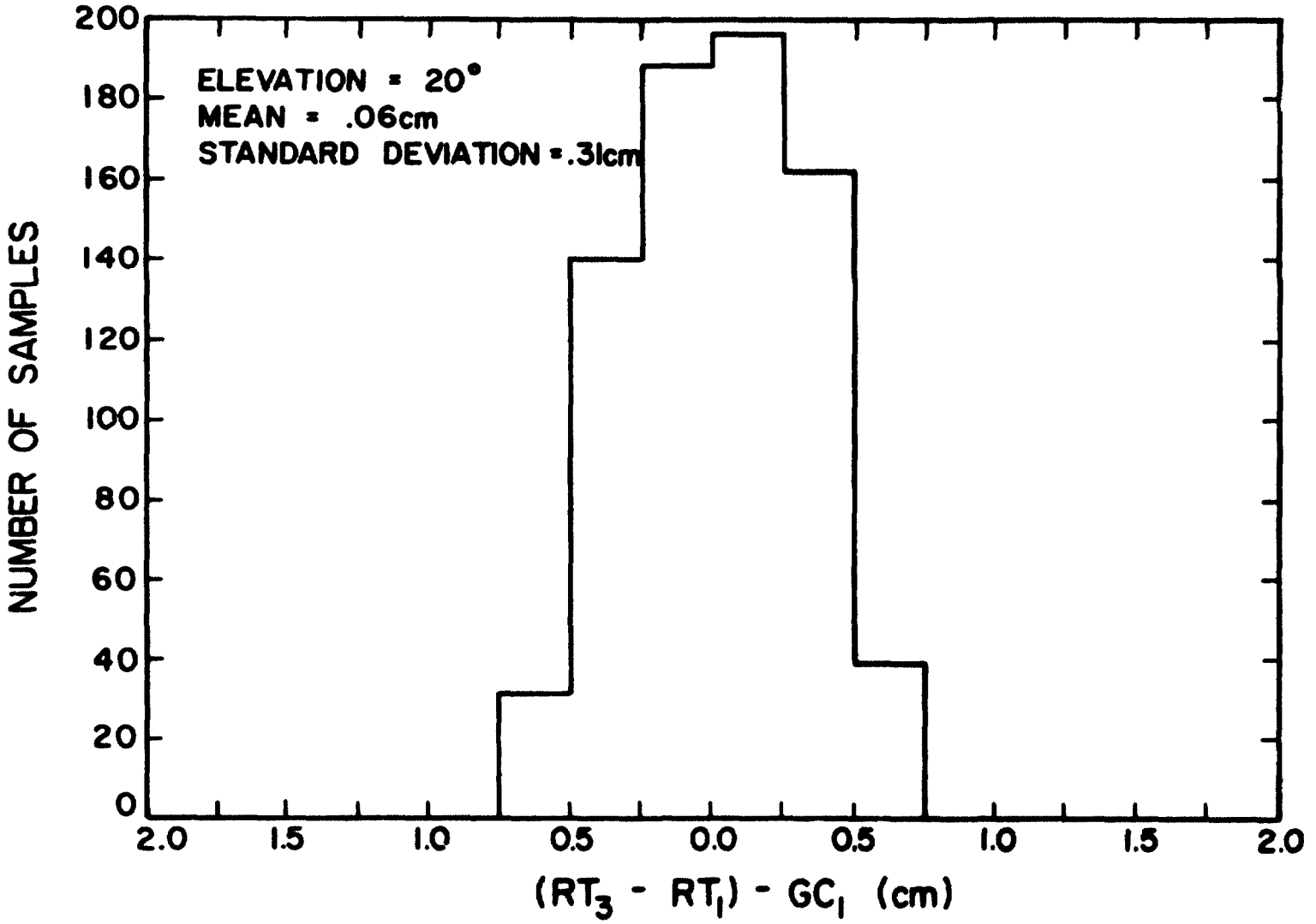

Figure 19. Histogram of residual gradient errors $(RT_3 - RT_1) - GC_1$. Elevation = 20°. Twenty-one data sets comprising Group A processed using Model a. Mean = .06 cm. Standard deviation = .31 cm.

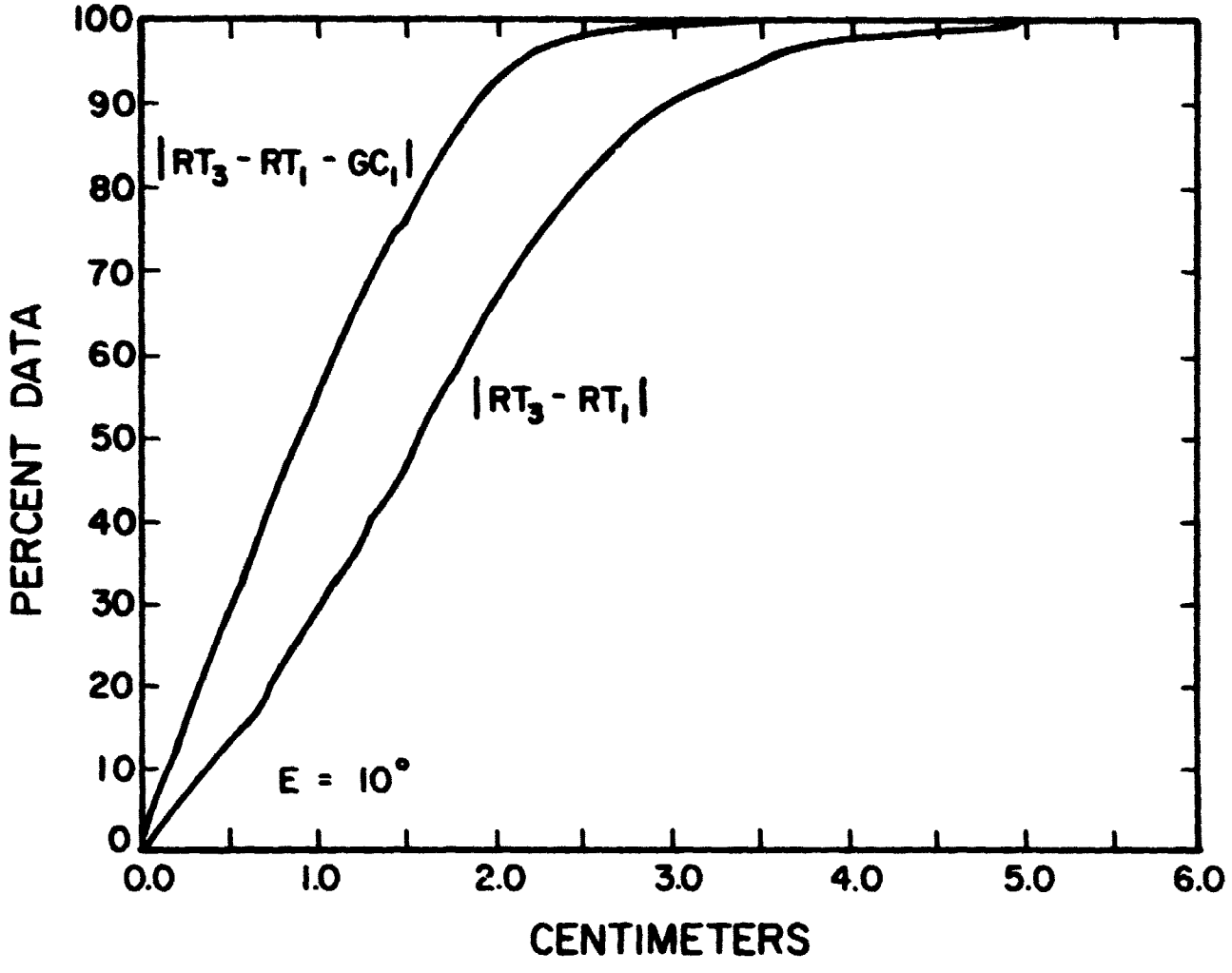

Figure 20. Percentage of errors less than the abscissa value before and after correction. Group/Model Aa (twenty-one data sets). Models are explained on page 78.

VI. EFFECTS OF RADIOSONDE MEASUREMENT ERRORS ON THE ACCURACY OF GC_1

Errors in surface measurements will of course introduce errors into the gradient correction term. The magnitude of these effects can be estimated from an analysis of the standard error of the regression coefficients which were used to obtain a least-squares fit of the surface data. The error is a function of the order of the regression polynomial and the locations of the surface weather stations. To illustrate the procedure we will calculate the error that would be expected using the Haven Hop radiosonde data.

The first term in GC_1 (2-22) is the most significant. Therefore the standard deviation of GC_1 can be approximated by

$$(GC_1)_{Std} \simeq \frac{C}{\sin E \tan E} \left[\frac{\partial}{\partial \rho} (P_s T_s K_s) \Big|_{\rho=0} \right]_{Std} . \qquad (6\text{-}1)$$

In the most general case the parameter $P_s T_s K_s$ is expanded in a two-dimensional m^{th} order regression polynomial

$$P_s T_s K_s = F = \sum_{k=1}^{m} \beta_k X_k \qquad (6\text{-}2)$$

where the X_k variables are the coordinate polynomials and the β_k are the regression coefficients. For a linear regression model we have

$$\begin{aligned} X_1 &= 1 & \beta_1 &= F_r \\ X_2 &= \theta & \beta_2 &= F_\theta \\ X_3 &= \phi \sin \theta & \beta_3 &= F_\phi \end{aligned} \qquad (6\text{-}3)$$

The derivative of $P_s T_s K_s$ can be related to the regression fit by (6-4).

$$\frac{\partial}{\partial \rho}\left(P_s T_s K_s\right)\Big|_{\rho=0} = \sum_{k=1}^{m} \beta_k \frac{\partial X_k}{\partial \rho}\Big|_{\rho=0} \quad . \tag{6-4}$$

The standard deviation of the derivative is related to the variances and covariances of the regression coefficients by (6-5).

$$\left[\frac{\partial}{\partial \rho}\left(P_s T_s K_s\right)\Big|_{\rho=0}\right]_{Std} = \left[\sum_{k=1}^{m}\sum_{\ell=1}^{m} C_{k\ell} \frac{\partial X_k}{\partial \rho}\frac{\partial X_\ell}{\partial \rho}\right]^{1/2}\Bigg|_{\rho=0} \tag{6-5}$$

where

$$C_{k\ell} = \text{cov}\ (\beta_k, \beta_\ell)$$
$$C_{kk} = \text{var}\ (\beta_k). \tag{6-6}$$

The regression coefficients are calculated by measuring $P_s T_s K_s$ at $n \geq m$ different weather stations. Let F_i be the i^{th} measurement of $P_s T_s K_s$ which is made at the coordinates $(X_{i1}, X_{i2}, \ldots, X_{im})$. Define $\underline{X}$ as the $n \times m$ matrix containing X_{ij} in its i^{th} row and j^{th} column.

$$\underline{X} = \begin{bmatrix} X_{11} & \cdots & X_{1m} \\ \vdots & & \vdots \\ X_{n1} & \cdots & X_{nm} \end{bmatrix} \quad . \tag{6-7}$$

Also define the column vectors

$$\underline{F} = [F_1, F_2, \ldots, F_n]^T$$
$$\underline{\beta} = [\beta_1, \beta_2, \ldots, \beta_m]^T \quad . \tag{6-8}$$

The least-squares regression solution for the $\underline{\beta}$ matrix is

$$\underline{\beta} = (\underline{X}^T \underline{X})^{-1} \underline{X}^T \underline{F} \quad . \tag{6-9}$$

The m × m variance-covariance matrix $\underline{C}$ for the regression coefficients is given by

$$\underline{C} = (\underline{X}^T\underline{X})^{-1}\,\sigma^2 \tag{6-10}$$

where σ is the standard measurement error of $P_sT_sK_s$, i.e., F.

In our analysis two-dimensional, first- and second-order regression polynomials were calculated for the parameter $P_sT_sK_s$. For simplicity we will consider only the linear regression fit. The matrix $\underline{X}^T\underline{X}$ is given by

$$\underline{X}^T\underline{X} = \begin{bmatrix} \sum_{k=1}^{n} X_{k1}^2 & \sum_{k=1}^{n} X_{k1}X_{k2} & \sum_{k=1}^{n} X_{k1}X_{k3} \\ \sum_{k=1}^{n} X_{k2}X_{k1} & \sum_{k=1}^{n} X_{k2}^2 & \sum_{k=1}^{n} X_{k2}X_{k3} \\ \sum_{k=1}^{n} X_{k3}X_{k1} & \sum_{k=1}^{n} X_{k3}X_{k2} & \sum_{k=1}^{n} X_{k3}^2 \end{bmatrix}. \tag{6-11}$$

The coordinates X_1, X_2 and X_3 are defined in (6-3). X_2 and X_3 are the horizontal displacements in the north-south and east-west directions. Since the radius of the earth is large, we can represent X_2 and X_3 approximately in polar coordinates with the origin taken as the location of site 54.

$$\begin{aligned} X_1 &= 1 \\ X_2 &= \rho \cos\alpha \\ X_3 &= \rho \sin\alpha \end{aligned} \tag{6-12}$$

where α is the azimuth angle of ρ. Note X_2 and X_3 are zero at site 54. If we let the n^{th} measurement of $P_sT_sK_s$ be taken at site 54, the $\underline{X}^T\underline{X}$ matrix

becomes

$$\underline{X}^T\underline{X} = \begin{bmatrix} n & \sum_{k=1}^{n-1} \rho_k \cos \alpha_k & \sum_{k=1}^{n-1} \rho_k \sin \alpha_k \\ \sum_{k=1}^{n-1} \rho_k \cos \alpha_k & \sum_{k=1}^{n-1} \rho_k^2 \cos^2 \alpha_k & \sum_{k=1}^{n-1} \rho_k^2 \cos \alpha_k \sin \alpha_k \\ \sum_{k=1}^{n-1} \rho_k \sin \alpha_k & \sum_{k=1}^{n-1} \rho_k^2 \cos \alpha_k \sin \alpha_k & \sum_{k=1}^{n-1} \rho_k^2 \sin^2 \alpha_k \end{bmatrix} . \tag{6-13}$$

The variance-covariance matrix $\underline{C}$ is fairly easy to calculate from (6-13) if we make some simplifying assumptions about the placement of the weather stations. For the Haven Hop data the stations are roughly located on the perimeter of a circle centered at site 54. If we let $\bar{\rho} = \frac{1}{n-1} \sum_{k=1}^{n-1} \rho_k$ and replace ρ_k by $\bar{\rho}$, (6-13) becomes

$$\underline{X}^T\underline{X} = \begin{bmatrix} n & \bar{\rho} \sum_{k=1}^{n-1} \cos \alpha_k & \bar{\rho} \sum_{k=1}^{n-1} \sin \alpha_k \\ \bar{\rho} \sum_{k=1}^{n-1} \cos \alpha_k & \bar{\rho}^2 \sum_{k=1}^{n-1} \cos^2 \alpha_k & \bar{\rho}^2 \sum_{k=1}^{n-1} \cos \alpha_k \sin \alpha_k \\ \bar{\rho} \sum_{k=1}^{n-1} \sin \alpha_k & \bar{\rho}^2 \sum_{k=1}^{n-1} \cos \alpha_k \sin \alpha_k & \bar{\rho}^2 \sum_{k=1}^{n-1} \sin^2 \alpha_k \end{bmatrix} . \tag{6-14}$$

If the stations are uniformly distributed along the circle perimeter and n is sufficiently large, the off-diagonal terms are approximately zero and summations in the diagonal terms are approximately $\frac{\bar{\rho}^2(n-1)}{2}$. In this case the variance-covariance matrix $\underline{C}$ is given by

$$\underline{C} = \begin{bmatrix} \frac{\sigma^2}{n} & 0 & 0 \\ 0 & \frac{2\sigma^2}{(n-1)\,\bar{\rho}^2} & 0 \\ 0 & 0 & \frac{2\sigma^2}{(n-1)\,\bar{\rho}^2} \end{bmatrix} . \qquad (6\text{-}15)$$

The standard error in GC_1 can now be calculated by substituting (6-15) into (6-5) and using the result in (6-1)

$$\text{Approx. } (GC_1)_{Std} = \frac{C}{\sin E \tan E} \sqrt{\frac{2}{n-1}} \frac{\sigma}{\bar{\rho}} \qquad (6\text{-}16)$$

where σ is the standard measurement error of $P_s T_s K_s$. σ can be expressed in terms of the standard errors of P_s and T_s.

$$\sigma = P_s T_s K_s \left[\frac{\sigma_p^2}{P_s^2} + \left(1 - \frac{1.04 \times 10^{-3} T_s}{K_s} \right)^2 \frac{\sigma_T^2}{T_s^2} \right]^{1/2} . \qquad (6\text{-}17)$$

Alternatively the error can be determined by evaluating (6-10) exactly using the locations of the radiosonde stations in the Project Haven Hop network.

From (6-1) and (6-5) the standard error in GC_1 is

$$(GC_1)_{Std} = \frac{C}{\sin E \tan E} \left[\sum_{k=1}^{m} \sum_{\ell=1}^{m} C_{k\ell} \frac{\partial X_k}{\partial \rho} \frac{\partial X_\ell}{\partial \rho} \right]^{1/2} \Bigg|_{\rho=0} . \qquad (6\text{-}18)$$

The coordinate polynomials X_k in (6-2) are

$$X_1 = 1 \qquad X_4 = \theta\phi\sin\theta$$
$$X_2 = \theta \qquad X_5 = \theta^2$$
$$X_3 = \phi\sin\theta \qquad X_6 = \phi^2\sin^2\theta \tag{6-19}$$

The coordinate matrix $\underline{X}$ (6-7) is calculated using the X_k's defined above evaluated at the colatitude and longitude of the radiosonde release sites. The colatitudes and longitudes are given in Appendix I. The $\underline{X}$ matrix is then used to evaluate the variance - covariance matrix $\underline{C}$.

$$\underline{C} = \left(\underline{X}^T\underline{X}\right)^{-1} \sigma^2 . \tag{6-20}$$

$\underline{C}$ has been calculated for the Haven Hop network and is given in Appendix I for linear, 4 coefficient, and quadratic models of $P_s T_s K_s$.

If we let the ranging site be 54 and

$$P_s = 1000 \text{ mb}$$
$$T_s = 275^\circ \text{ K}$$
$$K_s = .88913$$
$$\sigma_T = .7^\circ \text{ K}$$
$$\sigma_p = .7 \text{ mb}$$

and substitute these values into (6-17) we obtain

$$\sigma = 455.57.$$

The values of pressure, temperature, and K_s are typical of the Haven Hop data. The standard errors in pressure and temperature were obtained from Hoidale et al.[7]. Equation (6-18) requires the derivatives of the coordinate polynomials X_k with respect to ρ, evaluated at $\rho=0$.

From Appendix III they are

$$\left.\frac{\partial X_1}{\partial \rho}\right|_{\rho=0} = 0 \qquad (6\text{-}21)$$

$$\left.\frac{\partial X_2}{\partial \rho}\right|_{\rho=0} = \frac{-\cos\alpha}{r_e}$$

$$\left.\frac{\partial X_3}{\partial \rho}\right|_{\rho=0} = \frac{-\cos\alpha(\phi_o)\cos\theta_o + \sin\alpha}{r_e}$$

$$\left.\frac{\partial X_4}{\partial \rho}\right|_{\rho=0} = \frac{-\cos\alpha[\phi_o\sin\theta_o + \phi_o\theta_o\cos\theta_o] + \theta_o\sin\alpha}{r_e}$$

$$\left.\frac{\partial X_5}{\partial \rho}\right|_{\rho=0} = \frac{-2\theta_o\cos\alpha}{r_e}$$

$$\left.\frac{\partial X_6}{\partial \rho}\right|_{\rho=0} = \frac{-\cos\alpha(\phi_o)^2\sin 2\theta_o + 2\phi_o\sin\theta_o\sin\alpha}{r_e}$$

The derivatives of (6-21) are functions of azimuth. Therefore the estimated error, $(GC_1)_{Std}$, will have an azimuthal dependence. Equation (6-18) for the estimated error has been evaluated using the three models for $P_sT_sK_s$ and plotted as in Figures 21, 22, and 23. On the same graphs is the actual standard deviation of the residual errors Δ for Group Models Bc, Bd, and Bb, respectively. The value of $(GC_1)_{Std}$ averaged over all azimuths is given below for each model.

$$\overline{(GC_1)_{Std}}_{\text{linear}} = .45 \text{ centimeters}$$

$$\overline{(GC_1)_{Std}}_{\text{4 coefficient}} = .46 \text{ centimeters} \qquad (6\text{-}22)$$

$$\overline{(GC_1)_{Std}}_{\text{quadratic}} = .48 \text{ centimeters}$$

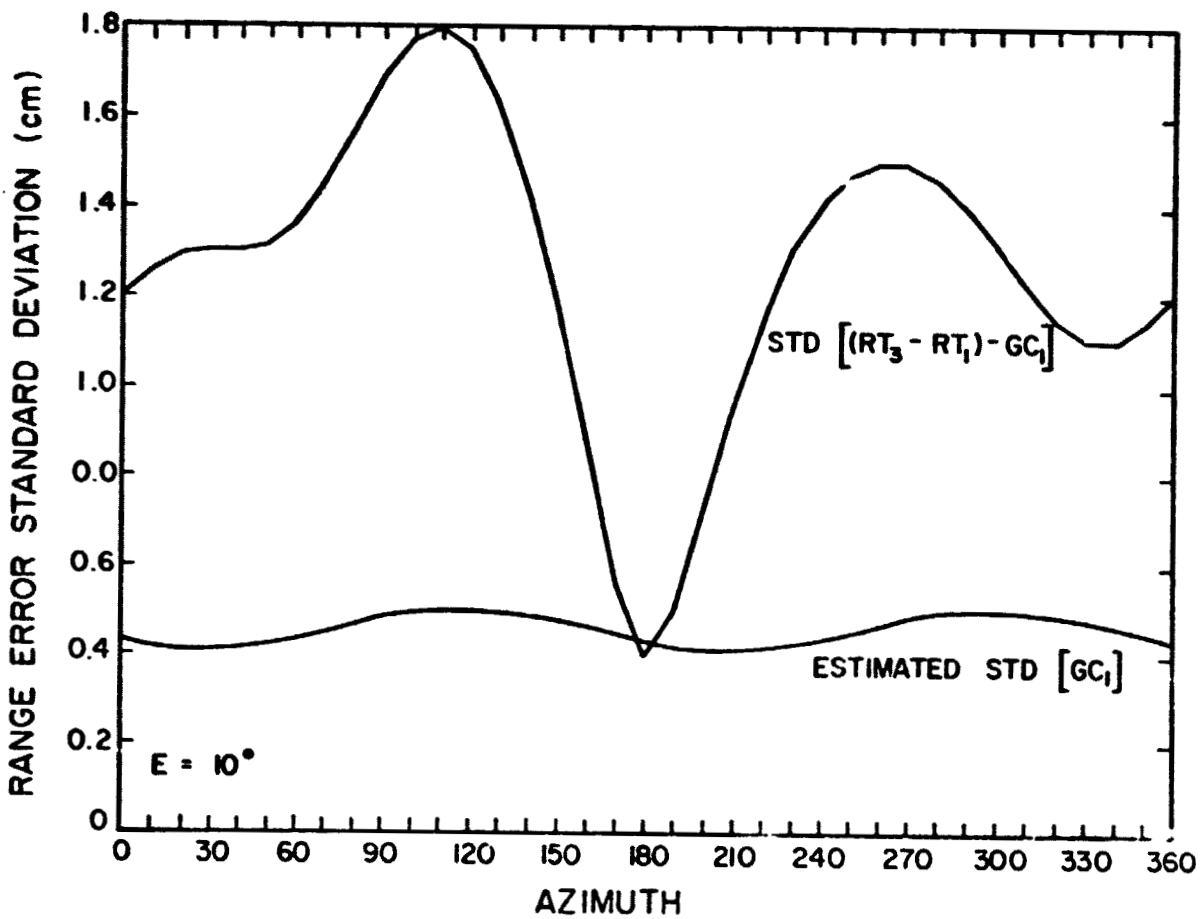

Figure 21. Standard deviation of $(RT_3 - RT_1) - GC_1$ nd the estimated standard deviation of GC_1 due to radiosonde measurement errors of .7°C and .7 mb versus azimuth. Elevation = 10°. Group B consisting of 10 arbitrary data sets from Group A processed using Model c (see page 78).

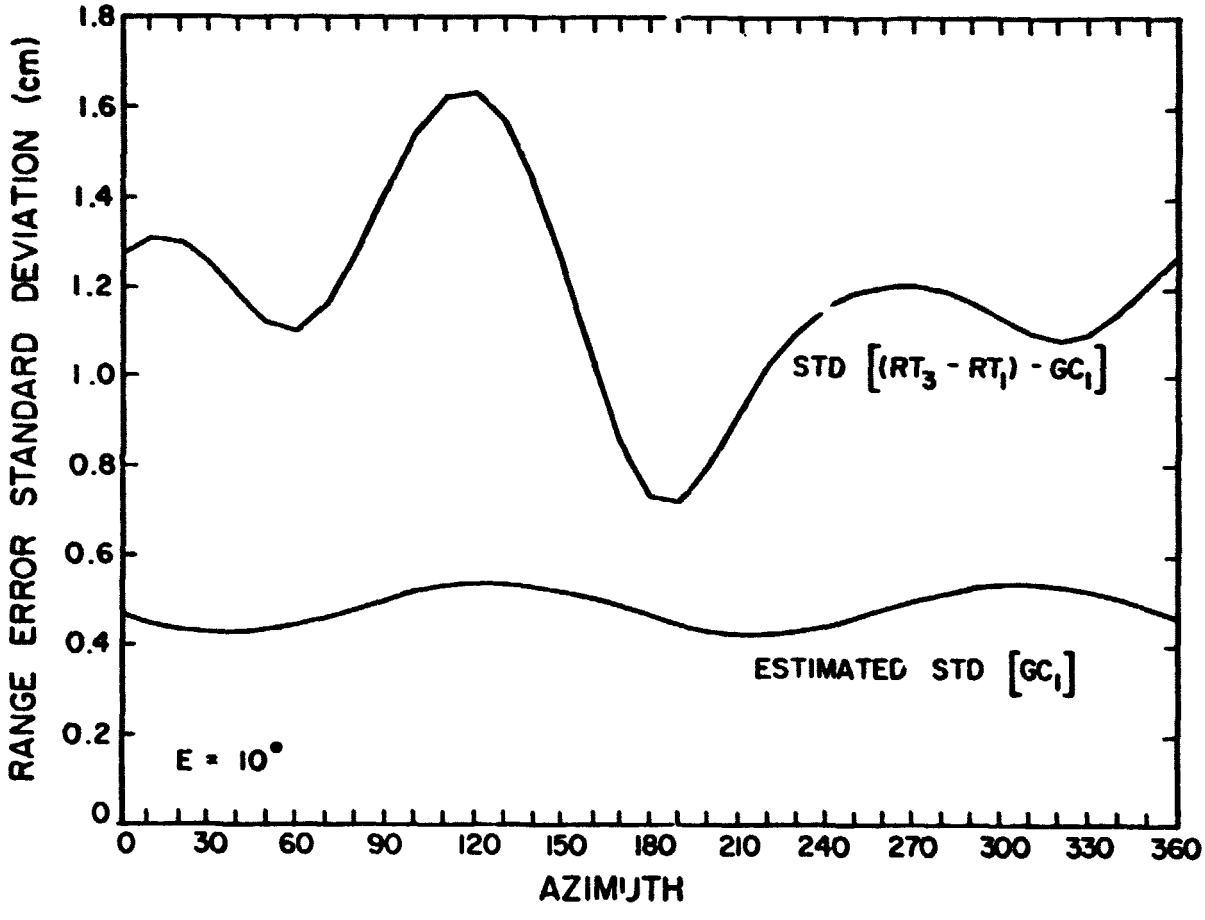

Figure 22. Standard deviation of $(RT_3 - RT_1) - GC_1$ and the estimated standard deviation of GC_1 due to radiosonde measurement errors of .7°C and .7 mb versus azimuth. Elevation = 10°. Group B consisting of 10 arbitrary data sets from Group A processed using Model d (see page 78).

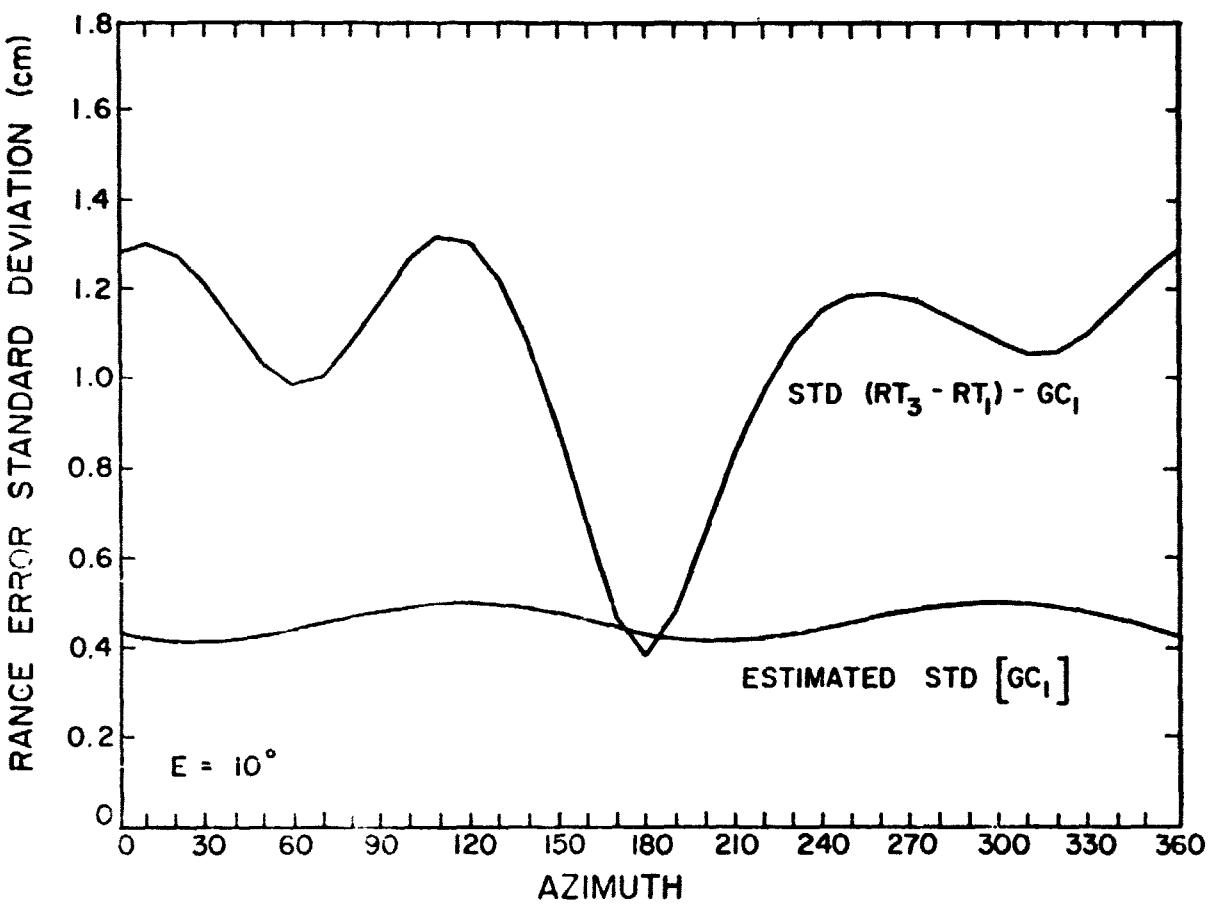

Figure 23. Standard deviation of $(RT_3 - RT_1) - GC_1$ and the estimated standard deviation of GC_1 due to radiosonde measurement errors of .7°C and .7 mb versus azimuth. Elevation = 10°. Group B consisting of 10 arbitrary data sets from Group A processed using Model b (see page 78).

The approximate value of $(GC_1)_{Std}$ for a linear model is given by (6-16). Letting $n = 8$

$\sigma = 455.57$

$\bar{\rho}$ = 140 kilometers = mean distance of sites 51 through 58 from site 54

$E = 10°$

the approximate error given by (6-16) is

$$\text{Approx. } (GC_1)_{Std} = .40 \text{ centimeters.} \tag{6-23}$$

If we neglect errors common to both the ray trace and GC_1, the total error (σ_Δ) in any evaluation of GC_1 may be divided into two parts. The first consists of errors in the formula itself (σ_F). The second contribution is due to errors in the radiosonde data (σ_D). Because the radiosonde data errors and the formula errors are uncorrelated, we can write

$$\sigma_\Delta^2 = \sigma_F^2 + \sigma_D^2 . \tag{6-24}$$

From the results of (6-22) σ_D is approximately .5 centimeters. The standard deviation of $\left[RT_3 - RT_1\right] - GC_1$, σ_Δ, from Tables 1 through 4, is approximately 1.1 centimeters. Substituting these values into (6-24), one finds $\sigma_F \simeq 1.0$ centimeters. This assumes the radiosonde data were in fact accurate to .7°C and .7mb. Changes in the accuracy of the radiosonde data will affect the accuracy of GC_1. In Figure 24 $(GC_1)_{Std}$ has been replotted for various values of the relative error in $P_s T_s K_s$. By referring to the 10, 20, or 40 degree elevation axis, it is possible to determine the errors in GC_1 due to radiosonde errors for any degree of radiosonde accuracy and elevation angle.

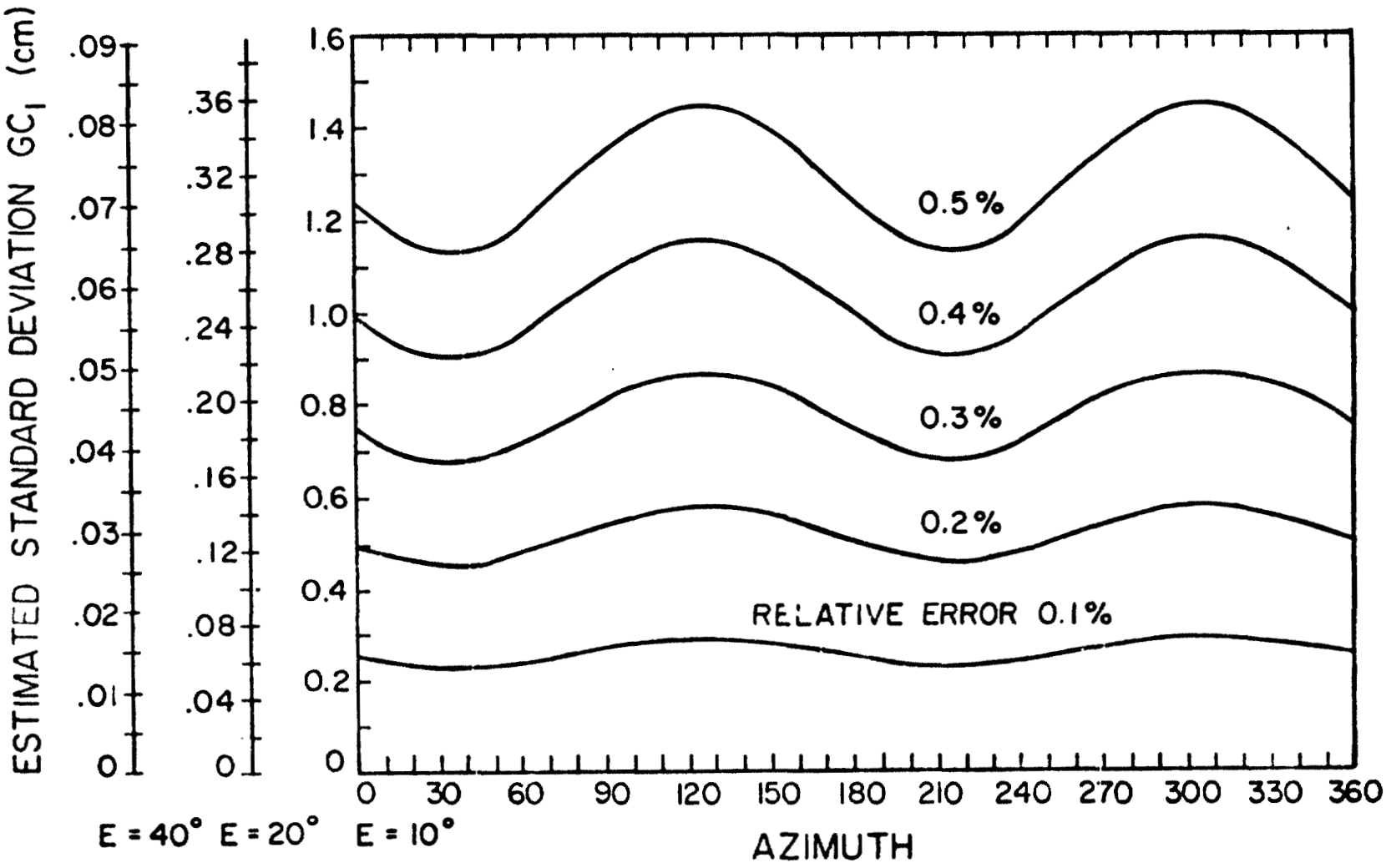

Figure 24. Standard deviation of GC_1 attributable to errors in the radiosonde data versus azimuth for several values of relative error in $P_s T_s K$

$$\left[\sigma_p^2 / p_s^2 + \sigma_T^2 / T_s^2 \left[1 - 1.04 \times 10^{-3} T_s / K_s \right]^2 \right]^{1/2}.$$

Elevation = 10, 20, and 40 degrees.

The values of σ_T and σ_P used in performing the above error analysis (.7° C and .7 mb) were obtained from Hoidale et al [7]. It is not clear that the Haven Hop data achieved this level of accuracy. From Figure 24, for σ_T = 1.3° C and σ_P = .7 mb, the errors in GC_1 due to radiosonde errors (σ_D) would approximately equal the residual errors found in our data ($\sigma_\Delta \simeq$ 1 cm). Thus a 1.3° temperature error could account for almost the entire residual error in the corrected data.

The pressure and temperature errors inherent in the Haven Hop data can be estimated by calculating the variance of the surface measurements about the regression polynomial. Using this approach and the 31 data sets in groups A, B and C, the pressure and temperature variances were estimated to be 0.8 mb and 1.3°C,respectively. The estimated pressure error is very close to the value reported by Hoidale et al.[7]. The estimated temperature error is almost twice as large as the value reported by Hoidale but appears to be realistic. Although actual instrumentation errors may be only 0.7°C, terrain features and ground cover variations could easily introduce an additional degree Centigrade or more error. Consequently, we believe the pressure errors in the Haven Hop data are close to the 0.7 mb value predicted by Hoidale while the temperature errors are close to the 1.3°C value which was estimated from the regression analysis.

GC_2 was evaluated to obtain a bound on the error introduced by the neglect of higher order terms in (2-8). Details of this evaluation are given in Appendix V. Variations in GC_2 were largely due to errors in the radiosonde data. In addition, little correlation was found between GC_2 and the residual errors $(RT_3 - RT_1) - GC_1$.

VII. CONCLUSIONS

A correction formula has been developed to correct laser ranging data for the effects of horizontal refractivity gradients. The formula requires the values of the horizontal pressure and temperature gradients at the laser site. The gradients can be determined by measuring the surface pressure and temperature at various locations around the ranging site and using polynomial regression to obtain a least squares fit to the surface data. The gradients can then be calculated directly from the regression polynomial.

The accuracy of the gradient correction formula was evaluated by comparing it with ray trace corrections. For a fixed elevation angle, the ray trace results indicate that horizontal refractivity gradients introduce refraction errors which are approximately sinusoidal functions of azimuth. The errors are minimum near 0° azimuth (due north) and maximum near 180° azimuth (due south). The average error has a peak-to-peak variation of approximately 5 centimeters at 10° elevation and approximately 1.25 centimeters at 20° elevation. The gradient correction formula is very effective in compensating for this sinusoidal bias error. The correction formula reduces the peak-to-peak value of the mean error to less than 1 centimeter at 10° elevation and less than 2 millimeters at 20° elevation.

When the gradient correction is applied to the ray trace data, the standard deviation of the residual error is approximately 1 centimeter at 10° elevation and 3 millimeters at 20° elevation. This residual error appears to be due almost entirely to errors in the meteorological data which are used to calculate the gradient correction term. The

residual error can be reduced either by using more accurate surface data or by employing additional weather stations to obtain a more accurate regression fit to the surface data. Temperature errors are the dominant factor in the gradient correction formula. If an adequate weather station network is not available, it may be sufficient to correct the ranging data by simply subtracting the bias err..:.

The analysis in this report did not consider the problem of extrapolating weather measurements to different altitudes. This could potentially be a major error source,particularly in mountainous regions such as California where weather stations may be located at widely different altitudes.

APPENDIX I.

DATA USED IN THE ERROR ANALYSIS OF SECTION IV

The coordinates of the radiosonde release sites used in evaluating the $\underline{X}$ matrix [Eq. (6-7)] are given below.

SITE	$\theta°$	$\phi°$
51	50.464	-76.227
52	51.000	-77.454
53	50.857	-75.464
54	51.643	-76.627
55	51.929	-78.136
56	52.500	-77.336
57	52.929	-76.345
58	52.072	-75.409

The variance-covariance matrices using the above site coordinates to evaluate Eq. (6-18) are given below for the linear, four-coefficient, and quadratic models.

Linear Variance-Covariance Matrix

$$\underline{C} = \begin{bmatrix} 549.13075 & -450.52012 & 136.01330 \\ -450.52012 & 1457.77028 & 823.79511 \\ 136.01330 & 823.79511 & 837.86486 \end{bmatrix} \sigma^2$$

Four-coefficient Variance-Covariance Matrix

$$\underline{C} = \begin{bmatrix} 3020051.7181 & -3358552.1110 & 2880027.4678 & -3202187.2600 \\ -3358552.1110 & 3736127.9583 & -3203011.0410 & 3561272.0384 \\ 2880027.4701 & -3202011.0430 & 2747573.3137 & -3054129.4350 \\ -3202187.263 & 3561272.0412 & -3054129.4360 & 3395924.6475 \end{bmatrix} \sigma^2$$

Quadratic Variance-Covariance Matrix

$$\underline{C} = \begin{bmatrix} 4726008. & -7183420. & 2840533. & 5162797. & 6980394. & 3578093 \\ -7183493. & 20023166. & 3525662. & -13856861. & -19130570. & -4292159. \\ 2840470. & 3525802. & 8464536. & -2096916. & -3157809. & 3128703. \\ 5163020. & -13857120. & -2096712. & 44644448. & 33624533. & 18191508. \\ 6980564. & -19130721. & -3157613. & 33624389. & 30132794. & 12957445. \\ 3578159. & -4292204. & 3128791. & 18191410. & 12957413. & 9309160. \end{bmatrix} \sigma^2$$

The four-coefficient and quadratic $\underline{X}^T\underline{X}$ matrices are ill-conditioned. Consequently computer round off errors have made them non symmetrical. The effects on the regression analysis are negligable.

APPENDIX II.

DISTANCE AND AZIMUTH TO LATITUDE AND LONGITUDE

Evaluation of GC_1 using Method II of Section II requires the determination of the latitude and longitude of an auxiliary site, Point 1, a given distance and azimuth from the ranging site, Point 0.

Let ϕ_o and ϕ_1 be the longitudes of Point 0 and 1 measured from the prime meridian. α is the azimuth of Point 1 relative to Point 0. Let θ_o and θ_1 be the colatitudes of Points 0 and 1. ρ_{o1} is the horizontal distance from Point 0 to Point 1 measured along the earth's surface.

From Figure II-1, C is the angle between Points 1 and 2 measured with respect to the center of the earth.

$$C = \frac{\rho_{o1}}{r_e}$$

where r_e is the radius of the earth. Using the law of cosines,

$$\cos \theta_1 = \cos \theta_o \cos \frac{\rho_{o1}}{r_e} + \sin \theta_o \sin \frac{\rho_{o1}}{r_e} \cos \alpha$$

$$\theta_1 = \cos^{-1} \left[\cos \theta_o \cos \frac{\rho_{o1}}{r_e} + \sin \theta_o \sin \frac{\rho_{o1}}{r_e} \cos \alpha \right].$$

Defining $\Delta\phi = \phi_1 - \phi_o$ and using the law of sines,

$$\frac{\sin \theta_1}{\sin \alpha} = \frac{\sin C}{\sin \Delta\phi}$$

$$\Delta\phi = \sin^{-1} \left[\frac{\sin \alpha}{\sin \theta_1} \sin \frac{\rho_{o1}}{r_e} \right]$$

$$\phi_1 = \Delta\phi + \phi_o$$

$$\phi_1 = \phi_o + \sin^{-1} \left[\frac{\sin \alpha}{\sin \theta_1} \sin \frac{\rho_{o1}}{r_e} \right].$$

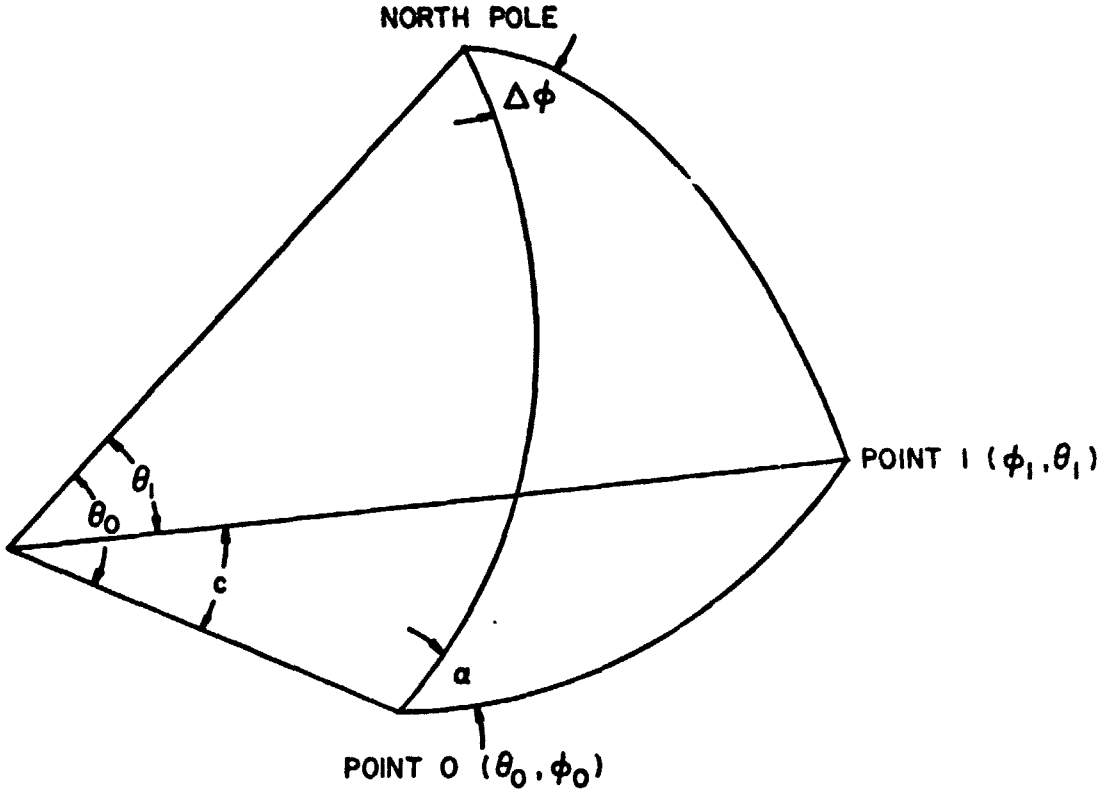

Figure II-1. Geometry used in expressing θ_1 and ϕ_1 as functions of ρ.

APPENDIX III.

EVALUATION OF $\frac{\partial F}{\partial \rho}$ AND $\frac{\partial^2 F}{\partial \rho^2}$

From Appendix II

$$\theta = \cos^{-1}\left[\cos\theta_o \cos\frac{\rho}{r_e} + \sin\theta_o \sin\frac{\rho}{r_e}\cos\alpha\right] \qquad \text{(III-1)}$$

$$\phi = \phi_o + \sin^{-1}\left[\frac{\sin\alpha}{\sin\theta}\sin\frac{\rho}{r_e}\right] \qquad \text{(III-2)}$$

where

θ_o = colatitude of ranging site

ϕ_o = longitude of ranging site

θ = colatitude of a point a distance ρ and azimuth α from the ranging site

ϕ = longitude of a point a distance ρ and azimuth α from the ranging site

r_e = radius of the earth

α = azimuth of point 1 relative to the ranging site.

Derivative of F-linear case

Let F be a polynomial expansion of the form (6-2). For the linear case

$$F = F_r + \theta \cdot F_\theta + \phi \sin\theta \cdot F_\phi \,. \qquad \text{(III-3)}$$

Using the chain rule

$$\frac{\partial F}{\partial \rho} = \frac{\partial F}{\partial \theta}\frac{\partial \vartheta}{\partial \rho} + \frac{\partial F}{\partial \phi}\frac{\partial \phi}{\partial \rho} \,. \qquad \text{(III-4)}$$

To determine $\left.\frac{\partial F}{\partial \rho}\right|_{\rho=0}$ it is necessary to calculate

$$\left.\frac{\partial F}{\partial \rho}\right|_{\rho=0} = \left(\left.\frac{\partial F}{\partial \theta}\right|_{\rho=0}\left(\left.\frac{\partial \theta}{\partial \rho}\right|_{\rho=0}\right) + \left(\left.\frac{\partial F}{\partial \rho}\right|_{\rho=0}\left(\left.\frac{\partial \phi}{\partial \rho}\right|_{\rho=0}\right)\right) \right. . \tag{III-5}$$

Using (III-1) and letting $x = \left(\cos\theta_o \cos\frac{\rho}{r_e} + \sin\theta_o \sin\frac{\rho}{r_e}\cos\alpha\right)$

$$\frac{\partial\theta}{\partial\rho} = \frac{\partial \cos^{-1}(x)}{\partial\rho} = \frac{-1}{(1-x^2)^{1/2}}\frac{\partial x}{\partial\rho} \tag{III-6}$$

$$\frac{\partial\theta}{\partial\rho} = -\left[1 - \left(\cos\theta_o \cos\frac{\rho}{r_e} + \sin\theta_o \sin\frac{\rho}{r_e}\cos\alpha\right)^2\right]^{-1/2} \cdot \left[\frac{-\cos\theta_o}{r_e}\sin\frac{\rho}{r_e} + \frac{\sin\theta_o\cos\alpha}{r_e}\cos\frac{\rho}{r_e}\right] \tag{III-7}$$

$$\left.\frac{\partial\theta}{\partial\rho}\right|_{\rho=0} = \frac{-\sin\theta_o\cos\alpha}{r_e}\left[1-\cos^2\theta_o\right]^{-1/2} \tag{III-8}$$

$$\left.\frac{\partial\theta}{\partial\rho}\right|_{\rho=0} = \frac{-\cos\alpha}{r_e} . \tag{III-9}$$

Using (III-2)

$$\frac{\partial\phi}{\partial\rho} = \frac{\partial}{\partial\rho}\sin^{-1}\left[\frac{\sin\alpha}{\sin\theta}\sin\frac{\rho}{r_e}\right]$$

$$= \left\{\frac{\sin\alpha}{\sin^2\theta}\left[\frac{1}{r_e}\left(\cos\frac{\rho}{r_e}\sin\theta - \cos\theta\,\frac{\partial\theta}{\partial\rho}\sin\frac{\rho}{r_e}\right)\right]\right\} \tag{III-10}$$

and letting $\rho = 0$

$$\left.\frac{\partial\phi}{\partial\rho}\right|_{\rho=0} = \frac{\sin\alpha}{r_e\sin\theta_o} . \tag{III-11}$$

$\frac{\partial F}{\partial\theta}$ and $\frac{\partial F}{\partial\phi}$ are determined using (III-3).

$$\left.\frac{\partial F}{\partial \theta}\right|_{\rho=0} = F_\theta + \phi_o \cos\theta_o \cdot F_\phi \qquad \text{(III-12)}$$

$$\left.\frac{\partial F}{\partial \phi}\right|_{\rho=0} = \sin\theta_o \cdot F_\phi \,. \qquad \text{(III-13)}$$

Substituting (III-13), (III-12), (III-11), and (III-9) into (III-4)

$$\left.\frac{\partial F}{\partial \rho}\right|_{\rho=0} = \frac{-\cos\alpha}{r_e}\left(F_\theta + \phi_o \cos\theta_o \cdot F_\phi\right) + \frac{\sin\alpha\, F_\phi}{r_e} \,.$$

Derivative of F-quadratic case

For the quadratic case let

$$F = F_r + \theta \cdot F_\theta + \phi \sin\theta \cdot F_\phi + \phi\theta \sin\theta \cdot F_{\theta\phi} + \theta^2 \cdot F_{\theta\theta} + \phi^2 \sin^2\theta \cdot F_{\phi\phi} \,. \qquad \text{(III-14)}$$

Using the chain rule (III-4) to differentiate (III-14)

$$\frac{\partial F}{\partial \rho} = \frac{\partial \theta}{\partial \rho}\left[F_\theta + \phi\cos\theta \cdot F_\phi + \phi\sin\theta \cdot F_{\theta\phi} + \phi\theta\cos\theta \cdot F_{\theta\phi} + 2\theta \cdot F_{\theta\theta} + \phi^2\, 2\sin\theta\cos\theta \cdot F_{\phi\phi}\right] + \frac{\partial \phi}{\partial \rho}\left[\sin\theta \cdot F_\phi + \theta\sin\theta \cdot F_{\theta\phi} + 2\phi\sin^2\theta \cdot F_{\phi\phi}\right] \,. \qquad \text{(III-15)}$$

Evaluating at $\rho = 0$ and using (III-11) and (III-9)

$$\left.\frac{\partial F}{\partial \rho}\right|_{\rho=0} = \frac{-\cos\alpha}{r_e}\left[F_\theta + \phi_o \cos\theta_o \cdot F_\phi + \phi_o \sin\theta_o \cdot F_{\theta\phi} + \phi_o\theta_o \cos\theta_o \cdot F_{\theta\phi} + 2\theta_o \cdot F_{\theta\theta} + \phi_o^2 \sin 2\theta_o \cdot F_{\phi\phi}\right] + \frac{\sin\alpha}{r_e}\left[F_\phi + \theta_o \cdot F_{\theta\phi} + \phi_o \sin\theta_o \cdot F_{\phi\phi}\right] \,. \qquad \text{(III-16)}$$

Evaluation of $\frac{\partial^2 F}{\partial \rho^2}$ -quadratic case

The chain rule may be applied again to (III-4) giving

$$\frac{\partial^2 F}{\partial \rho^2} = \frac{\partial^2 F}{\partial \theta^2}\left(\frac{\partial \theta}{\partial \rho}\right)^2 + 2\frac{\partial^2 F}{\partial \theta \partial \phi}\frac{\partial \phi}{\partial \rho}\frac{\partial \rho}{\partial \rho} + \frac{\partial F}{\partial \theta}\frac{\partial^2 \theta}{\partial \rho^2} + \frac{\partial^2 F}{\partial \phi^2}\left(\frac{\partial \phi}{\partial \rho}\right)^2 + \frac{\partial F}{\partial \phi}\frac{\partial^2 \phi}{\partial \rho^2}$$

where only nonzero terms have been retained. (III-17)

Letting $u = \frac{\sin \alpha}{\sin \theta_1} \sin \frac{\rho_{ol}}{r_e}$

$$\phi = \phi_o + \sin^{-1} u$$

$$\frac{\partial \phi}{\partial \rho} = (1 - u^2)^{-1/2}\frac{\partial u}{\partial \rho}$$

$$\frac{\partial \phi^2}{\partial \rho^2} = -\frac{1}{2}(1 - u^2)^{-3/2}(-2u)\left(\frac{\partial u}{\partial \rho}\right)^2 + \frac{\partial^2 u}{\partial \rho^2}(1 - u^2)^{-1/2}. \quad \text{(III-18)}$$

Evaluating (III-18) at $\rho = 0$, we obtain

$$\left.\frac{\partial^2 \phi}{\partial \rho^2}\right|_{\rho=0} = \frac{+2 \cos \theta_o \sin \alpha \cos \alpha}{r_e^2 \sin^2 \theta_o}. \quad \text{(III-19)}$$

Similarly

$$\left.\frac{\partial^2 \theta}{\partial \rho^2}\right|_{\rho=0} = \frac{1}{2}(1 - x^2)^{-3/2}(-2x)\left(\frac{\partial x}{\partial \rho}\right)^2 - \frac{\partial^2 x}{\partial \rho^2}(1 - x^2)^{-1/2}.$$

Evaluating at $\rho = 0$

$$\left.\frac{\partial^2 \theta}{\partial \rho^2}\right|_{\rho=0} = \frac{1}{2}\left|1 - \cos^2 \theta_o\right|^{-3/2}(-2 \cos \theta_o)\frac{\sin^2 \theta_o \cos^2 \alpha}{r_e^2} + \frac{\cos \theta_o}{r_e^2}\left|1 - \cos^2 \theta_o\right|^{-1/2}$$

$$= \frac{\cos \theta_o}{r_e^2 \sin \theta_o}(1 - \cos^2 \alpha).$$

$$\left.\frac{\partial^2\theta}{\partial\rho^2}\right|_{\rho=0} = \frac{\cos\theta_o \sin^2\alpha}{r_e^2 \sin\theta_o} \qquad \text{(III-20)}$$

When F is given as in (III-14), the other derivatives in (III-17) are as given below.

$$\left.\frac{\partial F}{\partial\theta}\right|_{\rho=0} = F_\theta + \phi_o \cos\theta_o \cdot F_\phi + F_{\theta\phi}[\sin\theta_o + \theta_o \cos\theta_o]\,\phi_o + 2\theta_o \cdot F_{\theta\theta} + \phi_o^2 \sin 2\theta_o \cdot F_{\phi\phi} \qquad \text{(III-21)}$$

$$\left.\frac{\partial^2 F}{\partial\theta^2}\right|_{\rho=0} = -\phi_o \sin\theta_o \cdot F_\phi + [2\cos\theta_o - \theta_o \sin\theta_o] \cdot F_{\theta\phi} + 2 \cdot F_{\theta\theta} + 2\phi_o^2 \cos 2\theta_o \cdot F_{\phi\phi} \qquad \text{(III-22)}$$

$$\left.\frac{\partial F}{\partial\phi}\right|_{\rho=0} = \sin\theta_o \cdot F_\phi + \theta_o \sin\theta_o \cdot F_{\theta\phi} + 2\phi_o \sin^2\theta_o \cdot F_{\phi\phi} \qquad \text{(III-23)}$$

$$\left.\frac{\partial^2 F}{\partial\phi^2}\right|_{\rho=0} = 2\sin^2\theta_o \cdot F_{\phi\phi} \qquad \text{(III-24)}$$

$$\left.\frac{\partial^2 F}{\partial\theta\partial\phi}\right|_{\rho=0} = \cos\theta_o \cdot F_\phi + \sin\theta_o \cdot F_{\theta\phi} + \theta_o \cos\theta_o \cdot F_{\theta\phi} + 2\phi_o \sin 2\theta_o \cdot F_{\phi\phi}. \qquad \text{(III-25)}$$

Substituting (III-9), (III-11), (III-19), (III-20), and (III-21 through 25) into (III-17) and collecting terms

$$\left.\frac{\partial^2 F}{\partial\rho^2}\right|_{\rho=0} = \frac{\cos^2\alpha}{r_e^2}\left[-\phi_o \sin\theta_o \cdot F_\phi + (2\cos\theta_o - \theta_o \sin\theta_o)\phi_o \cdot F_{\theta\phi} + 2 \cdot F_{\theta\theta} + 2\phi_o^2 \cos 2\theta_o \cdot F_{\phi\phi}\right]$$

$$- \frac{2\cos\alpha \sin\alpha}{r_e^2 \sin\theta_o}\left[\cos\theta_o \cdot F_\phi + \sin\theta_o \cdot F_{\theta\phi} + \theta_o \cos\theta_o \cdot F_{\theta\phi} + 2\phi_o \sin 2\theta_o \cdot F_{\phi\phi}\right]$$

$$+\frac{\cos\theta_o \sin^2\alpha}{r_e^2 \sin\theta_o}\left[F_\theta + \phi_o \cos\theta_o \cdot F_\phi + (\sin\theta_o + \theta_o\cos\theta_o)\phi_o \cdot F_{\theta\phi}\right.$$

$$\left. + 2\theta_o \cdot F_{\theta\theta} + \phi_o^2 \sin 2\theta_o \cdot F_{\phi\phi}\right]$$

$$+\frac{2\sin^2\alpha}{r_e^2} \cdot F\phi\phi$$

$$+\frac{2\cos\theta_o \cos\alpha \sin\alpha}{r_e^2 \sin\theta_o}\left[F_\phi + \theta_o \cdot F_{\theta\phi} + 2\phi_o \sin\theta_o \cdot F_{\phi\phi}\right] . \quad \text{(III-26)}$$

APPENDIX IV. FORM OF THE STANDARD DEVIATION OF GC_1

The standard deviation of GC_1 is determined using the first term of Eq. (2-22). The second term, which is much smaller, is neglected.

$$GC_1 = \frac{C}{\sin E \tan E} \frac{\partial}{\partial \rho} (P_s T_s K_s)\Big|_{\rho=0} . \qquad \text{(IV-1)}$$

For any modeling of $P_s T_s K_s$, GC_1 may be written as

$$GC_1 = G_N \cos \alpha + G_E \sin \alpha \qquad \text{(IV-2)}$$

where G_N is the north-south gradient correction and G_E is the east-west correction. The standard error in GC_1 can be written as

$$(GC_1)_{std} = \left(\sigma_N^2 \cos^2 \alpha + 2\sigma_{NE}^2 \cos \alpha \sin \alpha + \sigma_E^2 \sin^2 \alpha\right)^{1/2} \qquad \text{(IV-3)}$$

where

$$\begin{aligned} \sigma_N^2 &= \overline{G_N^2} - (\bar{G}_N)^2 \\ \sigma_E^2 &= \overline{G_E^2} - (\bar{G}_E)^2 \\ \sigma_{NE}^2 &= \overline{G_N G_E} - \bar{G}_N \bar{G}_E \end{aligned} \qquad \text{(IV-4)}$$

Equation (IV-3) can be simplified by assuming that G_N and G_E are uncorrelated and $\sigma_N^2 = \sigma_E^2$. It seems reasonable to assume that G_N and G_E are uncorrelated since the north-south gradient is primarily affected by seasonal variations in climate while the east-west gradient is essentially a diurnal effect. The Haven Hop data indicate this assumption is valid so that Equation (IV-3) can be written as

$$(GC_1)_{std} \approx \left(\frac{\sigma_N^2 + \sigma_E^2}{2}\right)^{1/2} \left[1 + \frac{\sigma_N^2 - \sigma_E^2}{\sigma_N^2 + \sigma_E^2} \cos 2\alpha\right]^{1/2} . \qquad \text{(IV-5)}$$

The Haven Hop data also indicate $\sigma_N \approx \sigma_E$ so that Equation (IV-5) can be approximated using the binomial theorem

$$(GC_1)_{std} \approx \left(\frac{\sigma_N^2 + \sigma_E^2}{2}\right)^{1/2} \left[1 + 1/2 \frac{\sigma_N^2 - \sigma_E^2}{\sigma_N^2 + \sigma_E^2} \cos 2\alpha\right] . \qquad \text{(IV-6)}$$

$(GC_1)_{std}$ is a sinusoid of frequency 2α where α is the azimuth angle. The form of (IV-6) may be compared with the standard deviation of GC_1 obtained using the data of Project Haven Hop I. In Fig. IV-1 the standard deviation of GC_1 for Group/Model Bd and an elevation of 10° has been plotted versus azimuth. From the figure it is clear the standard deviation of GC_1 contains sinusoidal variations at a frequency 2α superimposed on a constant bias level in agreement with (IV-6).

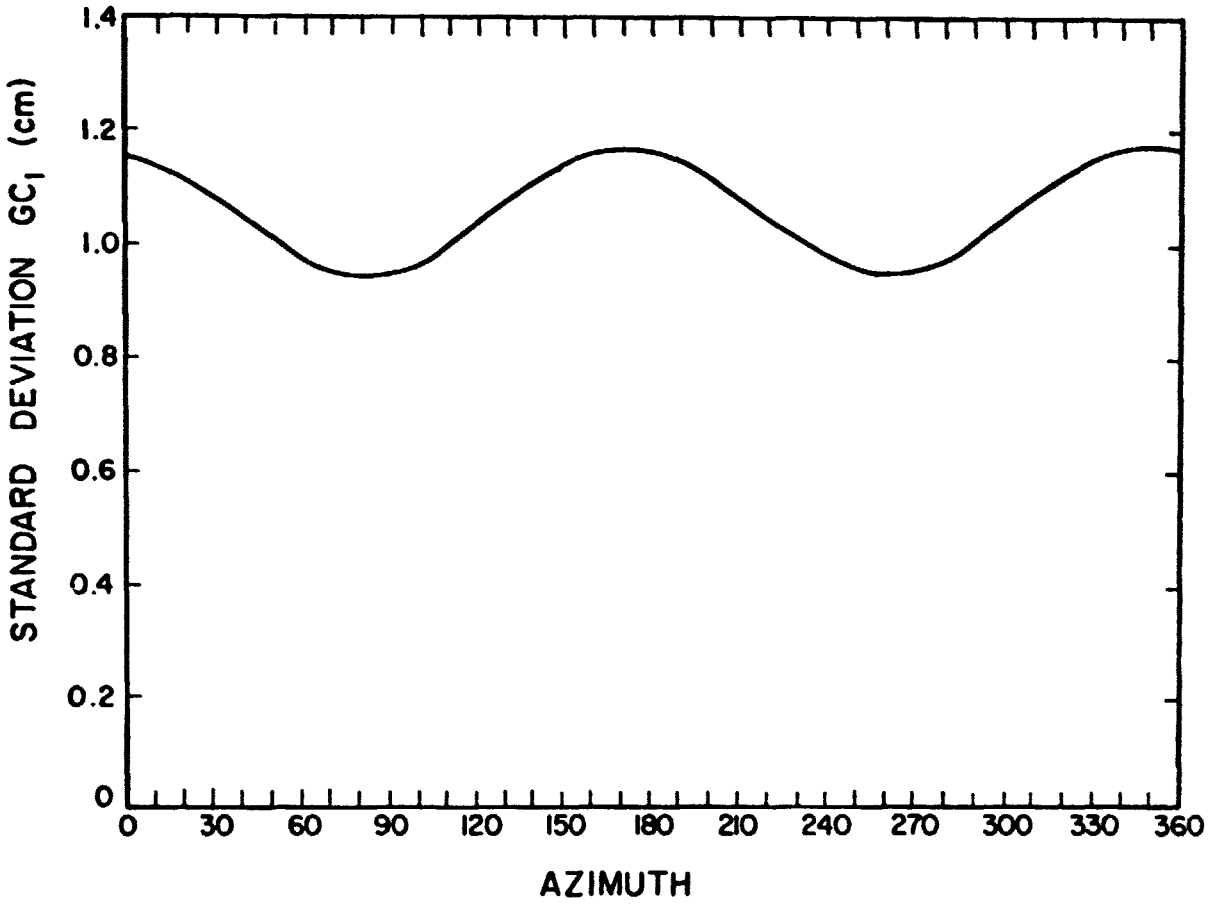

Figure IV-1. Standard deviation of GC_1 showing 2α variation. Group B. 10 data sets, Model d, E = 10°.

APPENDIX V. EVALUATION OF GC_2

An estimate of the error introduced into the gradient correction formula (2-8) by neglecting the higher-order terms of GC can be obtained by evaluating the second term in the series, GC_2.

$$GC_2 = \frac{2.029\ f(\lambda)}{\sin E \tan^2 E} \frac{\partial^2}{\partial \rho^2} \left(\frac{P_s T_s^2 K_s^2}{2 - K_s} \right) \Bigg|_{\rho=0} . \tag{V-1}$$

As in Section VI we can estimate the effect of errors in the radiosonde data. If we let

$$\sigma' = \frac{P_s T_s^2 K_s^2}{2 - K_s} \left(\frac{\alpha^2 \sigma_T^2}{T_s^2} + \frac{\sigma_p^2}{P_s^2} \right)^{1/2} \tag{V-2}$$

where

$$\alpha = 2 - 1.04 \times 10^{-3} \left(\frac{2T_s}{K_s} + \frac{T_s}{2 - K_s} \right),$$

then the estimated standard deviation of GC_2 is

$$(GC_2)_{\text{Std}} = \frac{2.029\ f(\lambda)}{\sin E \tan^2 E} \left[\sum_{k=1}^{m} \sum_{\ell=1}^{m} C_{k\ell} \frac{\partial^2 X_k}{\partial \rho^2} \frac{\partial^2 X_\ell}{\partial \rho^2} \Bigg|_{\rho=0} \right]^{1/2} . \tag{V-3}$$

Equations (V-1) through (V-3) were calculated for quadratic modeling of $\frac{P_s T_s^2 K_s^2}{2 - K_s}$ and

$$P_s = 1000 \text{ mb}$$

$$T_s = 275^\circ \text{ K}$$

$$K_s = .88913$$

$$\sigma_T = .7° \text{ K}$$

$$\sigma_p = .7 \text{ mb}$$

$$E = 10° .$$

The derivatives of the coordinate polynomials are available from Appendix III. The variance-covariance matrix $\underline{C}$ and the colatitude and longitude of the release sites are given in Appendix I.

GC_2 was evaluated using (V-1) and the radiosonde data of Group/Model Bd. For each azimuth the standard deviation of GC_2 was computed. The estimated standard deviation of GC_2 given by (V-3) and the actual standard deviation of GC_2 have been plotted versus azimuth in Figure (V-1). Both curves are on the same order of magnitude. This indicates errors in the radiosonde data are primarily responsible for variations in GC_2. The mean of GC_2 was approximately -4 mm. Figure V-2 shows GC_2 and $\Delta = (RT_3 - RT_1) - GC_1$ for data of 0930 1/26/70. The figure shows little correlation between GC_2 and the residual errors Δ.

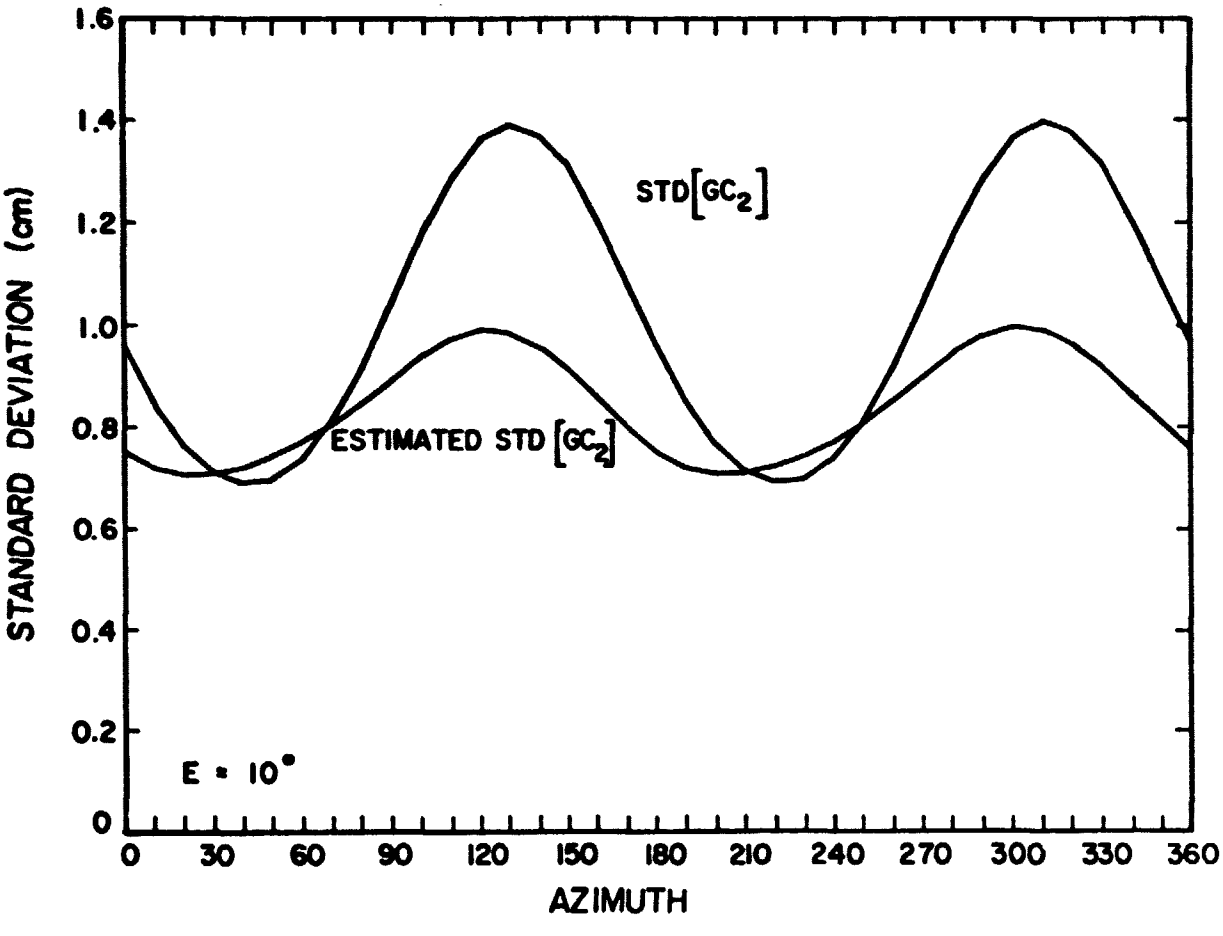

Figure V-1. Standard deviation of GC_2 calculated using Haven Hop data ($Std[GC_2]$) and the estimated standard deviation of GC_2 due to errors of .7°C and .7 mb in the radiosonde data versus azimuth. Group B (10 data sets). Model d. Elevation = 10°.

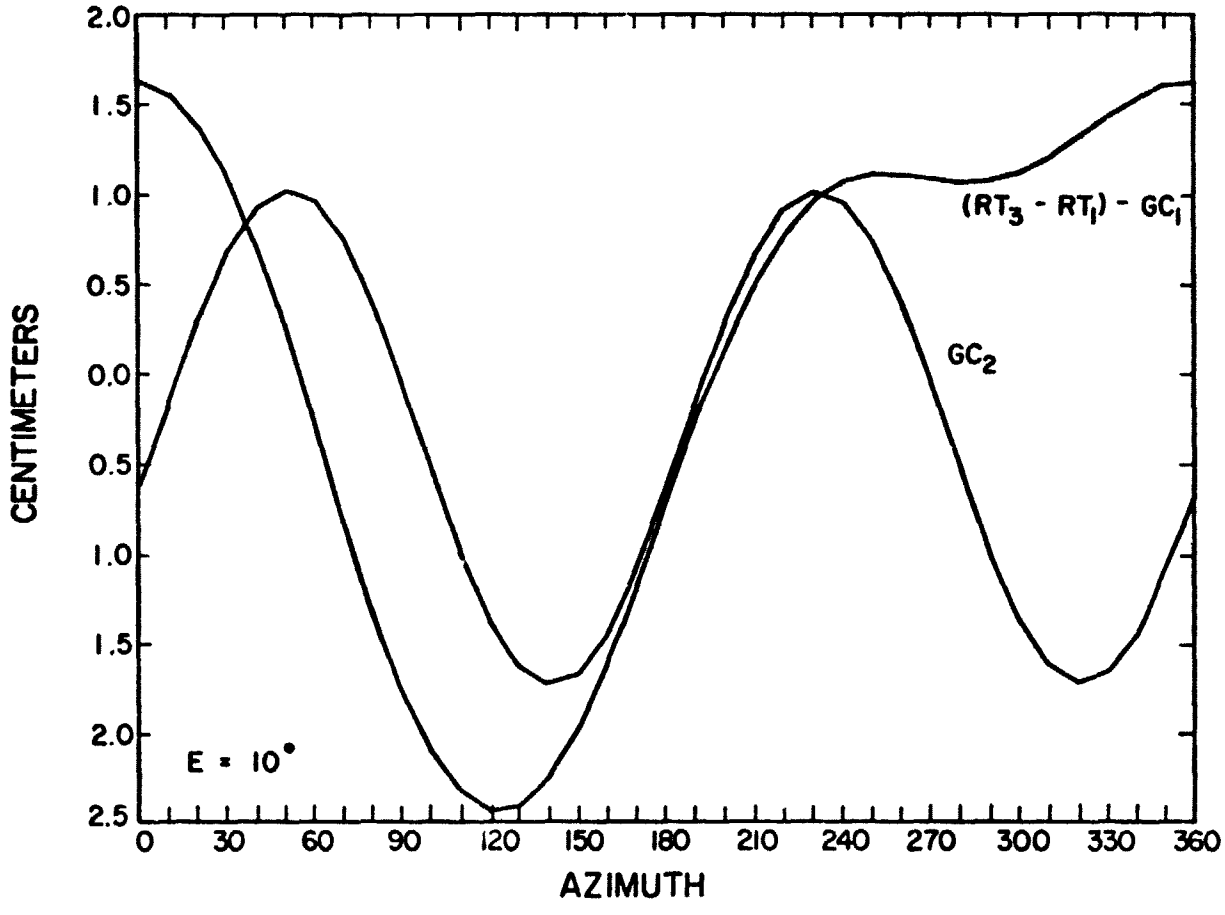

Figure V-2. GC_2 and $(RT_3 - RT_1) - GC_1$ versus azimuth. Data of 0930 1/26/70. Group B, Model d, E = 10°.

APPENDIX VI. SUMMARY OF PROCESSED DATA SETS AND MODELS

A brief summary of the processing methods is given in Table VI-1 below.

Table VI-1. Processing Methods and Data Sets of Section V.

Group/ Model	Number of data sets	Number of radio-sonde balloons	Regression model for surface data	Calculation of derivative	Ray trace refractivity model
Aa	21	8	Quadratic	Approximate Method I	Quadratic
Ba	10	8	Quadratic	Approximate Method I	Quadratic
Bb	10	8	Linear plus cross term	Approximate Method I	Linear plus cross term
Bc	10	8	Linear	Exact Method II	Quadratic
Bd	10	8	Quadratic	Exact Method III	Quadratic
Cb	10	7	Linear plus cross term	Approximate Method I	Linear plus cross term

REFERENCES

[1] J. J. Marini and C. W. Murray, "Correction of laser range tracking data for atmospheric refraction at elevations above 10 degrees," NASA Technical Report X-591-73-351, November 1973.

[2] Saastamoinen, J. "Atmospheric correction for the troposphere and stratosphere in radio ranging of satellites," Geophysical Monograph 15, "The use of artificial satellites for geodesy," American Geophysical Union, Washington, D. C., 1972.

[3] J. Marini, "Correction of satellite tracking data for an arbitrary tropospheric profile," Radio Science, vol. 7, pp. 223-231, 1972.

[4] D. L. Zanter, C. S. Gardner and N. N. Rao, "The effects of atmospheric refraction of the accuracy of laser ranging systems," RRL Publication No. 4[illegible] University of Illinois, Urbana, Illinois, January 1[illegible].

[5] S. Penn, G. J. Thompson, [illegible] and P. A. Giorgio, "Meteorological conditions associated [illegible] n CAT observations in Project Haven Hop," Air Force Surveys in Geophysics, No. 236, AFCRL-72-0043, Januar[illegible] 197[illegible].

[6] C. S. Gardner and J. R. Rowlett, "Atmospheric refraction errors in laser ranging systems," RRL Publication No. 477, University of Illinois, Urbana, Illinois, November [illegible].

[7] M. Hoidale, B. Gee and G. Harmon, "Atmospheric structure, White Sands Missile Range, New Mexico," Atmospheric Science Lab, White Sands Missile Range, DR-321, May 1968.